Chapter 1

Introduction

The chapter presents a short introduction to the thesis. The basic properties of plasmas in general and fusion plasmas are stated. Parameters of CASTOR and TEXTOR tokamak devices and plasmas are given.

1.1   Introduction to the thesis

This thesis presents a summary of the experimental results obtained during my PhD study at Faculty of Mathematics and Physics at Charles University in Prague. The most of the experimental work as well as training in the plasma physics theory was done in the Institute of Plasma Physics Association EURATOM/IPP.CR in Prague, which operates the CASTOR tokamak. The CASTOR tokamak is a small flexible device equipped with the unique set of probe diagnostics. Parameters of CASTOR plasmas are in many aspects similar to those measured at the plasma edge of the bigger devices, where the probes are used as well. Therefore, it is an ideal machine for development of novel probe diagnostics, fast and efficient testing of new ideas, and also training of young scientists.

The part of the thesis dedicated to the measurements of the magnetic field using Hall probes contains results obtained during my 3 months long stay in the Institute of Plasma Physics Association EURATOM-KFA Jülich on the TEXTOR tokamak. The TEXTOR is a middle size machine, oriented originally toward the study of plasma wall interactions but, with much broader range of interests in present including use of magnetic turbulence for controlled exhaust of particles and energy. Recently, spectroscopic methods for local measurements of the electrostatic turbulence in the plasma core are also developed here.

The resulting thesis are more a summary of different experimental approaches to the plasma turbulence than a single unique result. The emphasis is put on the magnetic turbulence, but some aspects of electrostatic turbulence are also studied, and the possible link between the both is envisaged. The plasma turbulence seems to be responsible for anomalously high transport of particles and energy out of the plasma. Despite the fact that this subject is extensively studied almost from the beginning of fusion plasma physics, it is still only partially understood. This thesis might be a small contribution to the effort to understand the turbulence in tokamaks.

1.2   Fusion plasma

Let's start with the definition of plasma in general. Plasma, sometimes said as the fourth state of matter, is in principle an ionized gas. More precisely, according to [1]:

Plasma is quasineutral ionized gas which shows a collective behaviour.

Let me discuss this definition in more details.

- Gas is quasineutral when it contains approximately the same number of positively and negatively charged particles and it's Debye length λ_D is much smaller than the typical dimension of the plasma. The Debye length is given by formula:

$$\lambda_D = \sqrt{\frac{\epsilon_0 k T_e}{n_e e^2}},\tag{1.1}$$

  where $\epsilon_0 = 8.85 \cdot 10^{-12}$ m^{-3}kg^{-1}s^{4}A^2 is dielectric constant, $k = 1.38 \cdot 10^{-23}$J/K is Boltzman constant, $e = 1.6 \cdot 10^{-19}$ C is electron charge, T_e is electron temperature in Kelvins and n_e is electron density in particles per meter cubed. The potential of an electrostatic charge e immersed into plasma is partially screened by the surrounding plasma charge carriers and decreases as [4]:

$$\varphi = \frac{e}{4\pi\epsilon_0 r} e^{-\sqrt{2}r/\lambda_D}.\tag{1.2}$$

Hence, the charge immersed into plasma can be considered as electrostaticaly screened by the plasma in the distance λ_D. In another words, at the scales larger than λ_D the plasma can be considered quasineutral. The typical dimensions of tokamak fusion plasmas are ranging from several centimeters up to a few meters. On the other hand the Debye length is of the order of tens of micrometers.
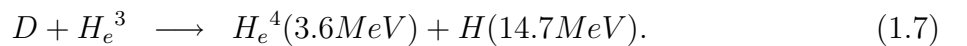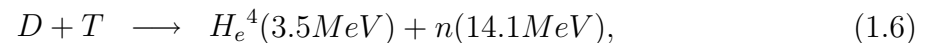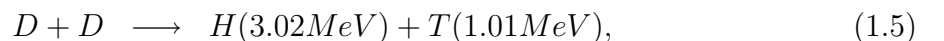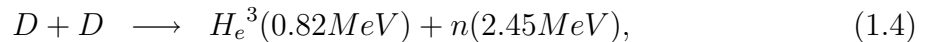
- Gas must be ionized in such extent that its properties are determined mainly by the electromagnetic forces and only in the minor way by the collisions with neutrals. The collisions of charged particles with neutrals are characterized by the collision frequency ν_N or by its inverted value, the averaged time between two subsequent collisions with the neutrals τ_N. The typical time scale for electrostatic interactions within the plasma is the frequency of electrostatic oscillations given by the plasma frequency ω_p given by:

$$\omega_p = \sqrt{\frac{ne^2}{\epsilon_0 m_e}}, \tag{1.3}$$

where m_e is the mass of electron. The similar equation is valid also for ions. These oscillations arise due to small misplacement of charged particles from equilibrium that cause the local breakdown of quasineutrality. The resulting electric field pull the particles back and drives the oscillating movement. The plasma frequency in fusion devices is usually high ~ 100 GHz. On the other hand, the collisions with neutrals are negligible, because plasma is almost fully ionized.

- The requirement of the collective behaviour of plasma implies that the large number of particles is involved in each plasma process. The smallest relevant volume in plasma is a sphere with radius of Debye length. The number of particles in this sphere is $N_D = n\frac{4}{3}\pi\lambda_D^3$. Consequently, the requirement of collective behaviour of a plasma can be expressed as $N_D \gg 1$. For illustration, for the CASTOR tokamak edge plasmas $N_D \approx 10^6$. The collective behaviour causes many difficulties in the mathematical description of plasma, but it is also the major source of the amusing variety of plasma processes.

The subject of this thesis is study of a special kind of plasmas called the fusion plasmas. The attribute 'fusion' means plasmas with such parameters that the plasma ions undergo nuclear fusion reactions forming the ions with higher atomic number. Clearly, an extremely high temperature ~ 10 keV[1] is necessary because fusing ions have to overcome their strong electrostatic repulsion. Moreover, the plasma has to be dense enough $\sim 10^{20}$ m^{-3}, and the particles and the energy has to be confined within the plasma volume for a sufficiently long time in order of several seconds. The plasma composed from ionized isotopes of hydrogen – deuterium or tritium, is of special interest, because in this case, the fusion nuclear reactions are strongly exothermic. Consequently, the ultimate goal of the fusion plasma physics is to built a commercial fusion power plant that will convert the excess energy of fusion burn into electricity. The relevant fusion reactions are:

$$D + D \longrightarrow H_e^3(0.82MeV) + n(2.45MeV), \tag{1.4}$$
$$D + D \longrightarrow H(3.02MeV) + T(1.01MeV), \tag{1.5}$$
$$D + T \longrightarrow H_e^4(3.5MeV) + n(14.1MeV), \tag{1.6}$$
$$D + H_e^3 \longrightarrow H_e^4(3.6MeV) + H(14.7MeV). \tag{1.7}$$

---

[1]$1eV = 1.6\ 10^{-19}J = 11600$K

Among these, the DT reaction (eq.1.6) can be reached most easily, therefore it is supposed to be used in the first generation of fusion power plants. The reactor based on DT reaction would burn naturally abundant deuterium. There is 33 g of D in each ton of ordinary water and the extraction technique is cheap.[2] The another input to the reactor is tritium, but in fact this will be bread in the closed cycle within the reactor's blanket from lithium, which is also abundant in the earth's crust and even more is dissolved in the see water. As a result, the fuel for the DT fusion reactors would cover our energy needs (at 1995 levels) for 60 million years. The energy is released in the form of neutrons that are absorbed in the reactor's lithium blanket. Their energy is converted into heat and finally into electricity using conventional power generating cycle. Abundant fuel, no atmospheric pollution, low radioactive waste and very high intrinsic safety make this concept an almost ideal long-term source of energy. The major draw-back is the extreme complexity af physical and technical aspects of this problem, which eludes solution, despite the worldwide coordinated efford of thousands of plasma physicists over the last five decades.

1.3   Tokamaks

Starting from early 50's several concept were suggested how to produce and confine fusion plasmas.[3] Naturally, the material containment is not possible due to extremely high temperature. Therefore, plasma has to be confined by special configuration of magnetic fields. Original attempts to trap plasmas in the linear tube between two magnetic mirrors were not very successful. Afterwards, closed magnetic devices and among them mainly tokamaks gained the priority in fusion research. The first tokamak (TOroidalnaja KAmera s MAgnitnymi Katuškami) was constructed in the middle of the fifth decade in the Soviet Union. In principle, every tokamak is a toroidal vessel where the plasma is confined by strong toroidal and poloidal magnetic fields. The toroidal plasma current is driven by transformer action. Plasma in the vessel acts as the secondary single-turn winding of a transformer. For more precise description of tokamak operation I have to start with some necessary geometry.
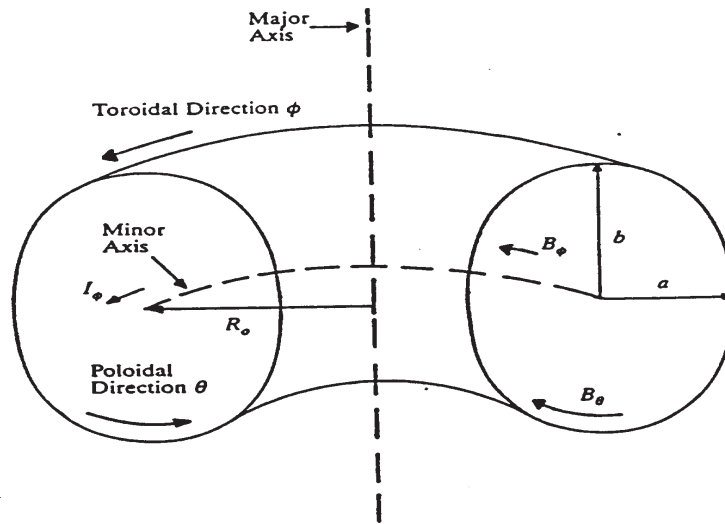

Figure 1.1: *Tokamak geometry.*

As you can see from Fig. 1.1, tokamak vessel is a torus with two axes of symmetry: major and minor. They characterize two basic directions: toroidal which is parallel to the minor axis and poloidal which is azimuthal to the minor axis. Another very important parameters of every tokamak are major and minor radii. Major radius is the shortest distance between major and minor axis. Minor radius is the shortest distance between the minor axis and the edge of the torus. Tokamaks are constructed with different poloidal cross-sections (circular, D-shaped, bean-shaped). Fig. 1.1 shows geometry of a tokamak with elliptical cross-section. Therefore, two minor radii a and b are needed to characterize its poloidal shape. In the most cases the cylindrical coordinates are used in mathematical models. In this models, every point inside the torus is given by three coordinates (z, θ, r), z is distance in toroidal direction, θ is angle in poloidal direction, and r is distance from the minor axis. Principal construction scheme of tokamak is in Fig. 1.2.
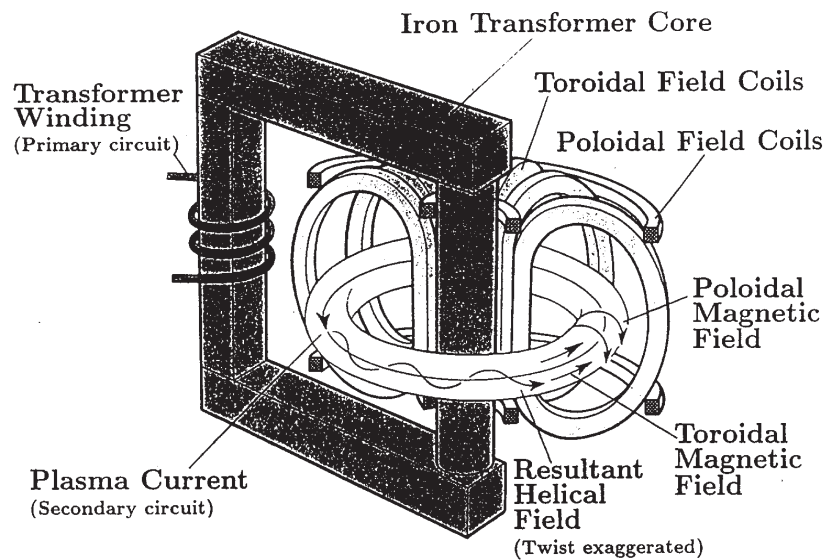

Figure 1.2: *Principal construction scheme of tokamak.*

It demonstrates transformer-like functioning of tokamak. The linearly increasing current in primary coils induces the electric field in toroidal direction inside the tokamak vessel. This field drives the plasma current I_p in toroidal direction and it is also responsible for ohmic heating of plasma. This toroidal plasma current also induces poloidal magnetic field B_θ. All around the tokamak vessel in poloidal direction are the coils of toroidal magnetic field B_T. Toroidal together with poloidal magnetic field creates helical field lines. This magnetic configuration helps to keep charged particles inside the torus. For stability of the plasma there are very important Helmholtz's (or mostly quadrupole) coils of vertical magnetic field B_V. Together with ExB drift they compensate the natural tendency of squeezed plasma column to stretch itself.

 The basic problems in tokamak operation are heating and confinement. The first idea was to gain ignition temperature by ohmic heating caused by plasma current I_p only. It is simply the Joule's heat $I_p^2 R$ dissipated into the plasma. Unfortunately, efficiency of this method decreases rapidly with gained temperature, because the plasma resistivity R decreases with increasing temperature. Therefore, other methods had to be introduced. I will mention the most common ones.

- **Neutral beam injection**: Ions are accelerated to high energy and then neutralized and injected inside the plasma. As the neutral particles trajectories are not affected by the tokamak magnetic field, the beam passes into the plasma and gradually, the neutral particles are ionised. The resulting high energy ions are confined by the magnetic field and deposit their energy on electrons and ions through collisions.

- **Ion cyclotron resonance heating (ICRH)**: ICRH relies upon the absorption of the fast ion cyclotron wave (few tens of MHz) by plasma ions. The wave frequency has to be in resonance with the frequency of ion cyclotron gyration around magnetic field lines.

- **Electron cyclotron resonance heating (ECRH)**: It works on the same principle as ICRH. The frequency of ECRH power generator has to be in resonance with plasma electron cyclotron frequency several tens of GHz. The energy is distributed to the plasma ions through the collisions.

- **Lower-hybrid heating**: The LH wave (a few GHz) can be absorbed by electrons or ions when their phase velocity matches the velocity of particle.

A some type of waves injected in plasma are able to drive an electric current. There are experiments where nearly whole current is driven by the waves. This could be solution for needed stationary tokamak operation, which is not possible in simple ohmic regime. The best results were obtained in the lower hybrid frequency range.

Several physical questions are still open. They are connected mainly with anomalous transport processes, alternative heating concepts and impurity control especially helium ash removal. Many technical problems connected mainly with the lack of suitable materials, that will withstand the immense neutron fluxes and magnetic fields without loosing its properties, still only wait for solution and sometimes may be even for recognition.

1.4   CASTOR Tokamak

Castor (Czechoslovak Academy of Sciences TORus) is a small, probably the oldest operational tokamak in the world. It has got its todays face after reconstruction of one of the first soviet tokamaks TM-1-MH. Here I will mention its basic parameters.

	central	edge (if different)
Circular cross-section with poloidal molybdenum limiter		
Major and minor radii R, a	0.4 m, 0.085 m	
Discharge duration	$\approx$ 40 ms	
Toroidal magnetic field B_T	up to 1.1 T	
Toroidal plasma current I_p	10 kA	
Safety factor q	usually ~ 2.5	~ 9
Ion and electron temperatures T_i, T_e	100 eV, 200 eV	10 eV, 10 eV
Plasma density n_e	$\approx 10^{19}\ m^{-3}$	$\approx 10^{18}\ m^{-3}$
Auxiliary heating	no	
Non-inductive current drive	LHCD at 1.25 GHz, 50 kW, up to 60% of I_p	
Particle and energy confinement time τ_P, τ_E	$\approx$ 1.2 ms, $\approx$ 0.5 ms	
Debye length λ_D	$\sim 30\ \mu$m	
Plasma frequency ω_p	180 GHz	60 GHz

Ion Larmour radius r_{Li}	1.5 mm	0.5 mm
Electron Larmour radius r_{Le}	50 μm	10 μm
Ion cyclotron frequency	15 MHz	
Electron cyclotron frequency ω_{ce}	30 GHz	
Mean free path λ	$\sim$ 100 m	
Repetition rate	up to $\sim$ 100 discharges/day	

Stuff (experiment) 4 senior scientists, 4 PhD + 1 MSc students, 4 support stuff

The toroidal magnetic field is measured using the coil winded around poloidal cross-section of the tokamak. The total plasma current is measured using Rogowski coil. Edge q is computed using formula (2.14) and central value of q according to (2.16). Electron temperature and density is measured at the plasma edge using Langmuir probes. The central value of T_e is deduced using the supposed profile:

$$T_e(r) = T_e(0)(1 - r^2/a^2)^{3/2} \tag{1.8}$$

Ion temperature is not measured routinely. The attempt was done to estimate it using neutral particle analyzer on CASTOR but, the data interpretation is not straightforward and it has not been finished yet. Line averaged density is measured using interferometer. The usually supposed density profile is:

$$n_e(r) = n_e(0)(1 - r^2/a^2) \tag{1.9}$$

Energy confinement time is deduced from diamagnetic measurements or estimated from global energy balance. The remaining quantities are computed according to the following formulas:

Electron or ion Debye length:
$$\lambda_D = 7.43 \ 10^3 \ \sqrt{\frac{T_{e,i}}{n}} \qquad [m, eV, m^{-3}], \tag{1.10}$$

Plasma frequency:
$$\omega_p = 56.4 \ \sqrt{n} \qquad [s^{-1}, m^{-3}], \tag{1.11}$$

Ion (hydrogen) Larmour radius:
$$r_{iL} = 0.144 \ \frac{\sqrt{T_i}}{B} \qquad [m, eV, T], \tag{1.12}$$

Electron Larmour radius:
$$r_{eL} = 3.38 \ 10^{-3} \frac{\sqrt{T_e}}{B} \qquad [m, eV, T], \tag{1.13}$$

Ion cyclotron frequency:
$$\omega_{ci} = 9.58 \ 10^7 \ B \qquad [s^{-1}, T], \tag{1.14}$$

Electron cyclotron frequency:
$$\omega_{ce} = 1.76 \ 10^{11} \ B \qquad [s^{-1}, T], \tag{1.15}$$

Mean free path:
$$\lambda = 4.5 \ 10^{17} \ \frac{T_{ei}^2}{n ln \Lambda} \qquad [m, eV, m^{-3}], \tag{1.16}$$
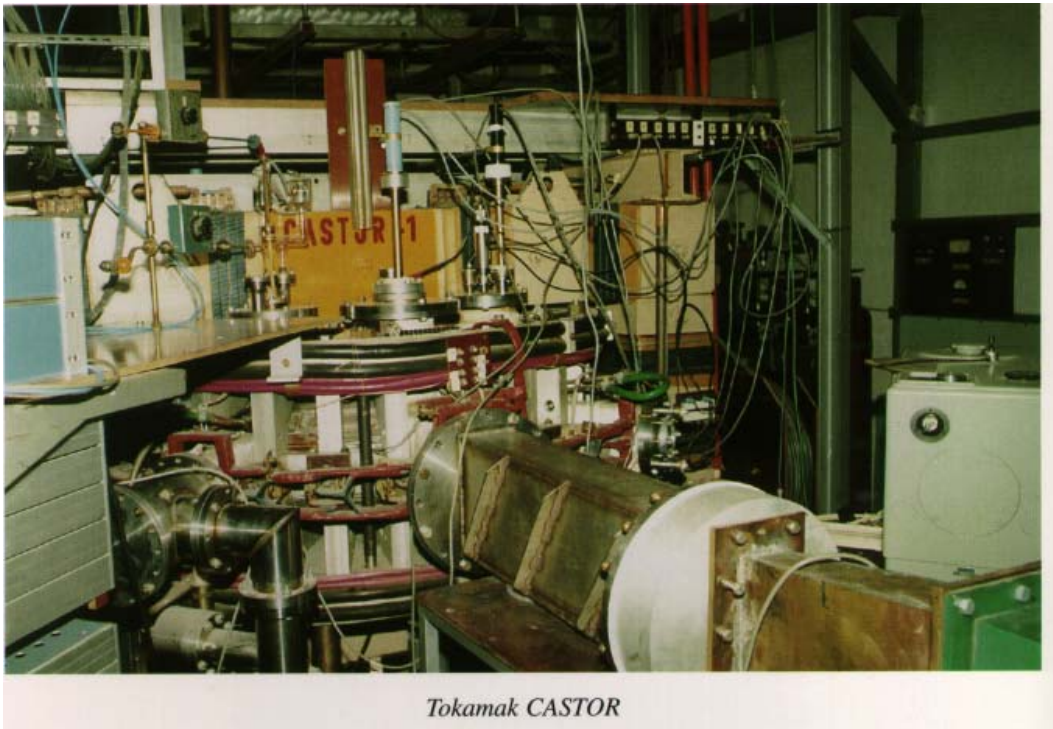
Tokamak CASTOR

Figure 1.3: *Side view of the CASTOR tokamak.*

1.5   TEXTOR tokamak

TEXTOR is a middle size tokamak operated by the Institute of Plasma Physics Association EURATOM-KFA Jülich, Germany. It has been used for and extensive campaign of research into the deposition of low Z materials on to plasma facing surfaces. The initial experiments introduced carbonization (carbon deposition over the entire surface of the inner wall). This led to significant reduction of impurity release from the walls with reduction factors 5–8 for oxygen and 10–20 for metals. Improved techniques of boronization and siliconization led to further improvements in TEXTOR performance.

The careful measurements of the current density profile on TEXTOR using Faraday rotation had an crucial impact on understanding of large MHD instability phenomena as sawtooth collapse.

The concept of toroidal pump limiter allowed improved control of the density and the study of exhaust of injected helium and gaseous impurities. The problem of avoiding the excessive heat loads at the leading edge of the pump limiter has been overcome by generating a cold radiative plasma boundary employing injected neon as radiating impurity. Up to 90% of the total power has been radiated from the plasma boundary in stable and quasi–stationary discharges without degradation of energy confinement (written according to [4]). Recently, the new supplementary system Dynamic Ergodic Divertor (DED) was put into operation on TEXTOR to improve confinement and controlled exhaust features of TEXTOR. DED creates a layer of ergodic magnetic field in the edge plasmas efficiently distributing the power loads over larger area of plasma facing components.

The main parameters of TEXTOR tokamak device and plasmas are summarized in the following table.

Circular cross-section, toroidal pump limiter and dynamic ergodic divertor

Major and minor radii R, a	1.75 m, 0.46 m
Toroidal field B_T	1.3 – 2.9 T
Plasma current I_p	200 – 800 kA
Pulse duration	< 10 s
Edge safety factor q	3.8 (standard operation)
Plasma density n_e	$\approx 5 \times 10^{18}$ m^{-3}
Ion and electron temperatures T_i, T_e (OH)	1 keV, 1 keV
Ion and electron temperatures T_i, T_e (Aux. H)	2 keV, 4 keV
Energy confinement time	tens of milliseconds
Ohmic heating	0.3 – 0.5 MW
NBI heating	2 × 1.5 MW
ICRH heating	2 × 2.2 MW
ECRH heating	400 kW in 200 ms
planned	1 MW in 3 s
Repetition rate	∼ 40 shots/day

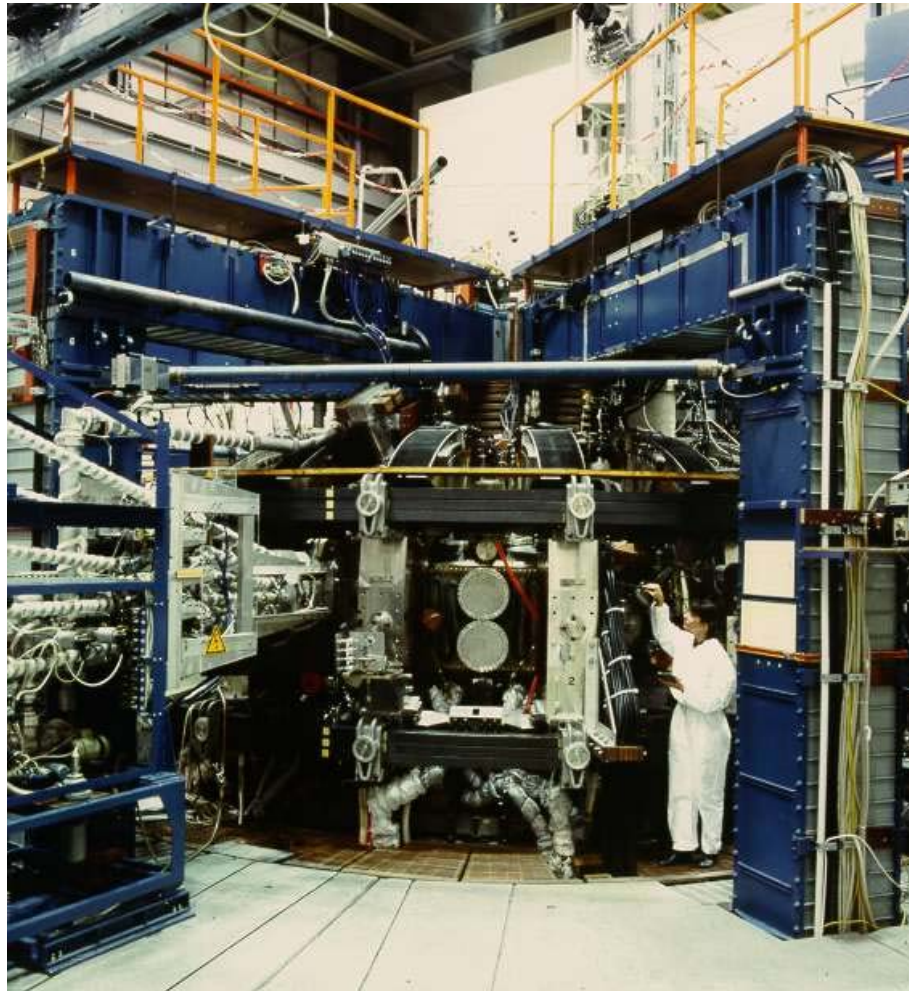Stuff (D-part of TEC) 40 Drs +10 PhD students + 60 support stuff

Figure 1.4: Side view of the TEXTOR tokamak.

Chapter 2

Magnetic field in tokamak

This chapter reviews the basic configuration of magnetic field in the tokamak with material limiter. The arrangement of magnetic field in the CASTOR tokamak is shown as an example. Geometry of magnetic field lines is described. Bases of Magneto-Hydro-Dynamic (MHD) description of the fusion plasmas is presented. Stability of the magnetic configuration of tokamak is discussed. The main instabilities are reviewed with emphasis on tearing modes. Finally, the transport caused by magnetic turbulence is estimated.

2.1   Introduction

Configuration of magnetic field is crucial for stability of the tokamak plasma column. Toroidal curvature of magnetic field lines together with electric fields create a very complex system, that is subject to several drifts and instabilities. The full description of this system involves determination of the velocity distribution functions for each plasma specie in every time instance using Boltzmann equation coupled with the full set of Maxwell's equations. This description is for many purposes too cumbersome. Therefore, the magneto-hydro-dynamic (MHD) approximation is often used. Here, the plasma is treated as a single fluid interacting with the electromagnetic field. Because of the fluid approach, this approximation describes well the global macroscopic effects but, fails in description of individual particles.

In the following, the configuration of magnetic fields of the CASTOR tokamak is described. Then, a brief introduction to the MHD theory is given. Examples of the MHD instabilities appearing in the tokamak plasmas are shown. Their influence on particle and heat fluxes is estimated.

2.2   Magnetic configuration in tokamak

2.2.1   Toroidal magnetic field

Toroidal magnetic field in tokamak is created by external coils turned poloidally around the vacuum vessel. There is 28 toroidal field coils each with 11 turns at CASTOR with total inductance L=2.8 mH. Discharging capacitor battery with capacitance C=0.23 F charged up to 2 kV into this inductance (current up to 20 kA) results in induction of sinusoidal damped toroidal magnetic field B_T with the peak value of 1.2 T and the half period $\tau_{1/2} = \pi\sqrt{LC} \approx 80$ ms. The plasma discharge is usually triggered from 30 – 50 ms after beginning of B_T.
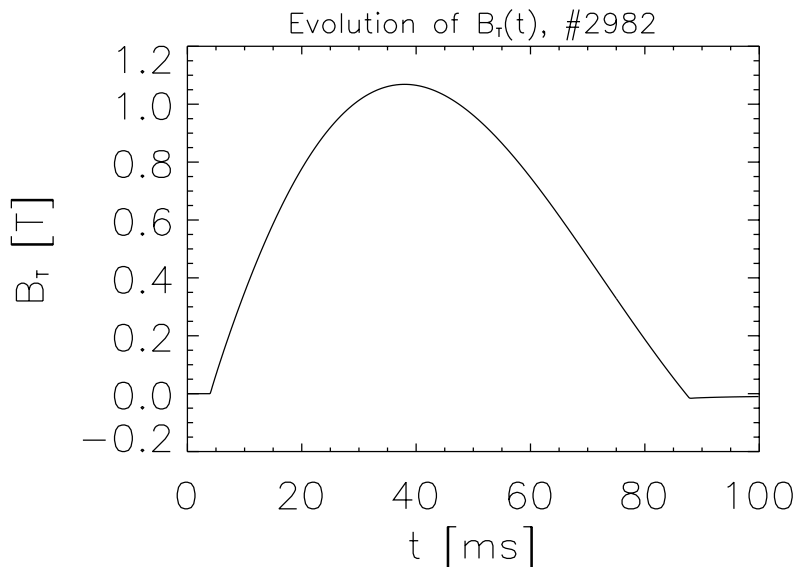

Figure 2.1: The time evolution of the toroidal magnetic field. Note that B_T is not constant over the duration of the CASTOR discharge. In the bigger devices, the current to the toroidal field coils is kept constant for the duration of plasma to ensure constant B_T.

Taking the center of coordinate system to be in the center of plasma column, the B_T decays with distance from tokamak major axis as:

$$B_T(r) = \frac{\mu_0}{2\pi} \frac{NI}{r + R_0},\tag{2.1}$$

where I is current flowing through the toroidal field coils, N is the total number of windings, and R_0 is the major radius. Radial decay of B_T in CASTOR is demonstrated in the figure 2.2 in the poloidal cross-section.
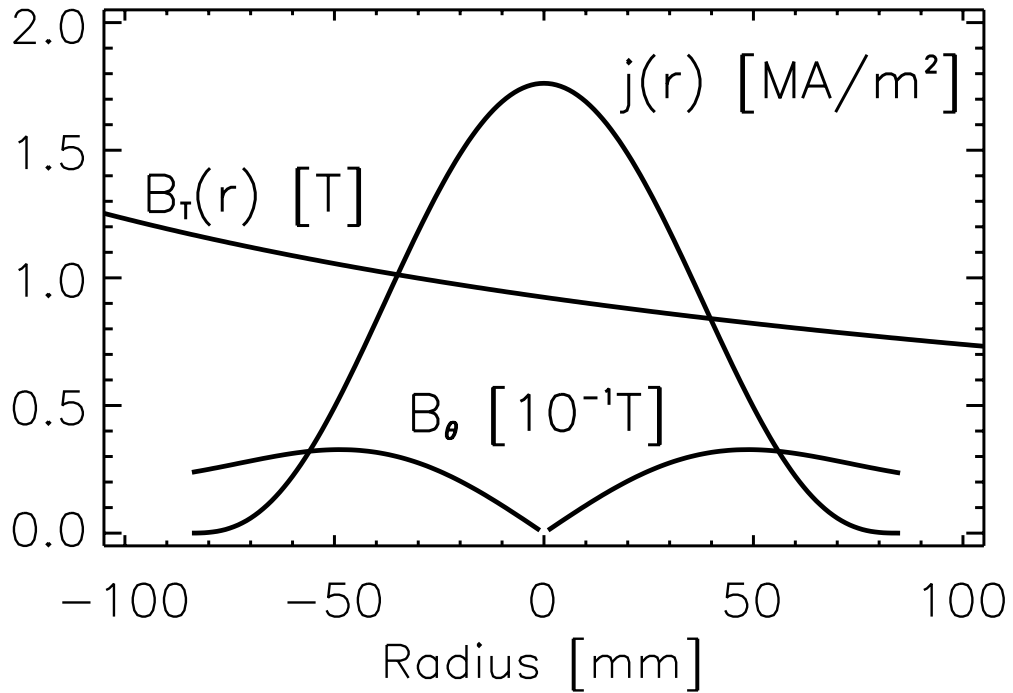

Figure 2.2: Radial profile of the toroidal magnetic field, plasma current density and the poloidal magnetic field for typical discharge parameters of the CASTOR tokamak. Negative values of the radius indicate locations closer to the tokamak major axis - high field side (HFS)

Plasma diamagnetism

Larmour gyration of charged plasma particles around the magnetic field lines is in such direction that the magnetic field induced by this gyration lowers the background magnetic field. In another words, plasma is diamagnetic. Because of this natural plasma diamagnetism, the B_T is slightly lower within the plasma volume than the value computed from the current in the toroidal field coils (vacuum field). Besides computing the vacuum field from the current flowing through the toroidal field coils, it can be directly measured using the set-up presented in the Fig. 2.3.
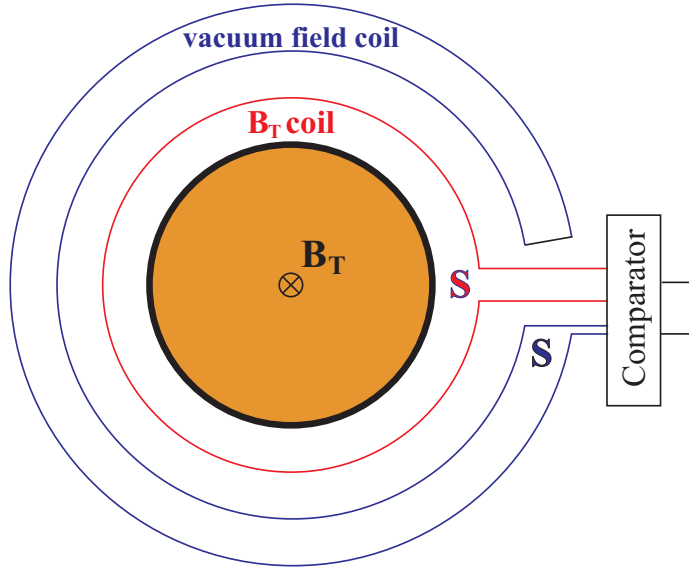
Figure 2.3: Schematic arrangement of the typical experiment measuring plasma diamagnetism. The figure shows the poloidal cross-section of the tokamak. The vacuum and the B_T coils must have exactly the same area S.

The same area of the B_T and the vacuum coil ensures the zero difference signal (output of the comparator) in the discharges without the plasma. In the discharge with plasma, the difference signal $\Delta\Phi$ is given by two terms [5]:

$$\Delta\Phi = \Delta\Phi_I - \Delta\Phi_{dia} = \frac{\mu_0^2}{8\pi B_T}I_p^2 - \frac{\mu_0}{B_T}W_\perp. \tag{2.2}$$

The diamagnetic term $\Delta\Phi_{dia}$ is the change of toroidal magnetic flux due to the plasma diamagnetism. Additional effect that changes the amplitude of B_T is caused by plasma current flowing along helical field lines – there is a poloidal component of plasma current flow. This poloidal component of the current changes the toroidal magnetic flux by $\Delta\Phi_I$. $W_\perp$ is perpendicular particles energy content per unit of length, The perpendicular plasma energy $W_\perp$ is related to the plasma thermal energy W_{th} by:

$$W_{th} = \frac{3}{2}W_\perp 2\pi R, \tag{2.3}$$

and consequently the energy confinement time can be deduced using:

$$\tau_E = \frac{W_{th}}{P_\Omega}, \tag{2.4}$$

where P_Ω is a ohmic heating power input to the tokamak plasma. It is given by the product of plasma current and the voltage drop toroidaly along the plasma column, measured by the single loop turned toroidaly around the torus.

2.3   Poloidal magnetic field

The poloidal component of the magnetic field B_θ is induced by the toroidaly flowing plasma current I_p. The radial profile of $B_\theta(r)$ is given by the radial profile of the plasma

current density. According to Ampére's law $B_\theta(r)$ is directly proportional to the total current $I(r)$ flowing through the closed circle with center in the center of the plasma column and diameter r.

$$B_\theta(r) = \frac{\mu_0}{2\pi} \frac{I(r)}{r}. \tag{2.5}$$

As the experimental data about the current profile are usually missing, $I(r)$ will be estimated assuming the current density profile $j(r)$ as follows:

$$j(r) = j(0)(1 - \frac{r^2}{a^2})^p, \tag{2.6}$$

where $j(0)$ is current density in the center of the plasma column and p is the peaking factor. This type of profile arises from the temperature (and consequently conductivity) profile that peaks in the plasma column center and falls down toward the plasma edge. $I(r)$ is now computed as a double integral of $j(r)$ from 0 to r and over the whole poloidal angle.

$$
\begin{aligned}
I(r) &= j(0) \int_0^r dr' r' (1 - r'^2/a^2)^p \int_0^{2\pi} d\theta \\
&= 2\pi j(0) \frac{a^2}{p+1} [1 - (1 - r^2/a^2)^{p+1}].
\end{aligned}
\tag{2.7}
$$

Putting $r = a$, the central current density $j(0)$ is derived:

$$j(0) = \frac{p+1}{\pi a^2} I(a). \tag{2.8}$$

Hence, $I(r)$ can be estimated as:

$$I(r) = I(a)[1 - (1 - r^2/a^2)^{p+1}]. \tag{2.9}$$

Finally, the radial profile of B_θ is:

$$B_\theta(r) = \frac{\mu_0}{2\pi} \frac{I(a)}{r}[1 - (1 - r^2/a^2)^{p+1}]. \tag{2.10}$$

Example of typical profiles of plasma current density and poloidal magnetic field are shown in Fig. 2.2.

2.4 Horizontal & vertical magnetic fields

Because of toroidal curvature, the poloidal magnetic pressure $p_{B_\theta} = \epsilon_0 c^2 B_\theta^2/2$ is stronger at the inner side of the torus – high field side (HFS – stronger B_T), than on the low field side (LFS). It results in tendency of plasma column to stretch itself. Therefore, additional magnetic field in vertical direction B_v has to be applied to compensate this effect and ensure stability of plasma column. Orientation of B_V has to be so that the resulting $j \times B_V$ force acts in the inward direction. Coils producing horizontal magnetic field B_H arranged similarly as for B_V can be used to position the plasma column vertically using $j \times B_H$ drift. Currents to the vertical and horizontal magnetic field coils is usually feed-back controlled in real time to ensure stability of the plasma column in both directions during the whole discharge. Schematic diagram of the vertical and horizontal magnetic field coils in CASTOR tokamak is in the Fig. 2.4
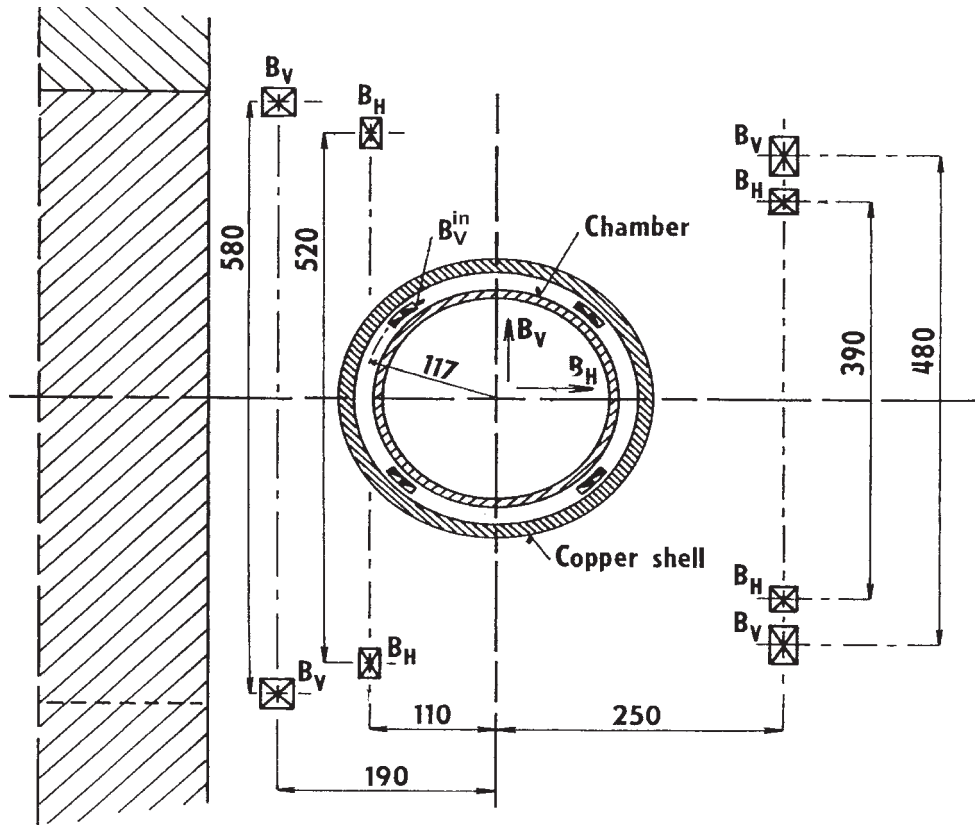
Figure 2.4: Configuration of horizontal and vertical magnetic field coils in the CASTOR tokamak. Here the inner B_V^{in} coil imposes a predefined (derived from the signal of plasma current) compensation of the horizontal plasma drift while, B_V and B_H coils serve for fast (¡ 10 kHz) on-line feed-back control of the vertical (unipolar) and horizontal (bipolar) plasma position.

2.5   Magnetic surfaces in tokamak – safety factor

The magnetic field in tokamak can be described in terms of magnetic surfaces. Each magnetic field line is in ideal case helix and it lays on a surface called magnetic surface. In the ideal case the magnetic surfaces in tokamak form the number of tori with different minor radii – Fig. 2.5(a).

Figure 2.5: Ideally nested (a), and more realistic magnetic surfaces in tokamak (b).

However, in the real case the situation is different compared to that displayed in Fig. 2.5(a). Due to the MHD (magnetohydrodynamic) instabilities (mainly resistive - tearing modes), the structure of magnetic surfaces is broken down and reestablished in the way that so called magnetic islands are formed on the magnetic surfaces with rational values of safety factor $q(r_s) = m/n$. Here, the m denotes poloidal and n toroidal mode numbers of the instability. The magnetic surfaces in poloidal cross-section resemble more those displayed in Fig. 2.5(b). Here, only the biggest magnetic islands at $q = 1$ and $q = 2$ are displayed. For description of magnetic surfaces the quantity called safety factor q is very important parameter. Safety factor q is defined as:

$$q = \frac{\Delta\varphi}{2\pi}. \tag{2.11}$$

The meaning of this parameter can be simply explained as follows. The magnetic field line follows a helical path as it travels round the torus on its associated magnetic surface. If at some toroidal angle φ, the field line has a certain position in the poloidal plane, it will return to exactly the same position in the poloidal plane after change of toroidal angle $\Delta\varphi$. For a large aspect ratio tokamaks with the circular cross-section the expression for q is approximately:

$$q(r) = \frac{r}{R} \frac{B_T}{B_\theta(r)}, \tag{2.12}$$

where B_T is a toroidal magnetic field, $B_\theta(r)$ is a poloidal magnetic field and r, R are the minor and major radius. The aspect ratio is defined as $\epsilon = R/a$, where a is the minor radius. The criterion of large aspect ratio tokamak $\epsilon \gg 1$ is fulfilled for CASTOR tokamak ($\epsilon = 4.7$). Using already derived expression for $B_\theta(r)$ the q(r) as a function of measurable plasma parameters total plasma current I_p and toroidal magnetic field B_T is given by:

$$q(r) = q(a)\frac{r^2/a^2}{1 - (1 - r^2/a^2)^{p+1}}, \tag{2.13}$$

where $q(a)$ denotes the safety factor at the limiter position.

$$q(a) = \frac{2\pi}{\mu_0} \frac{a^2}{R} \frac{B_T}{I(a)} \tag{2.14}$$

The following formula is valid for $q(a)$ for Castor tokamak with $a = 85mm$:

$$q(a) = 90.3\frac{B_T}{I(a)} \qquad\qquad [T, kA]. \tag{2.15}$$

A relatively simple relation bounds together $q(0)$, $q(a)$ and p:

$$\frac{q(0)}{q(a)} = \frac{1}{p+1}. \tag{2.16}$$

Next figure shows profiles of $j(r)$ and $q(r)$ for typical CASTOR tokamak plasma parameters and for a few reasonable values of the peaking factor p.
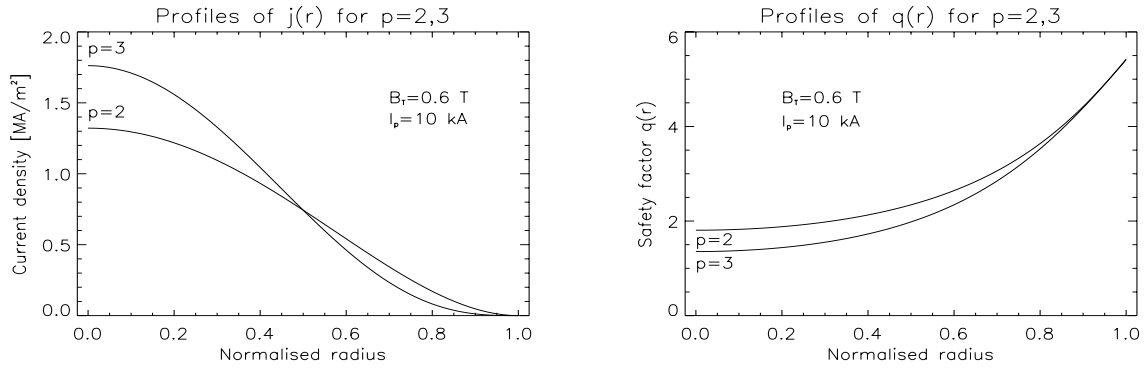
Figure 2.6: j(r) and q(r) profiles for I_p=10 kA, B_T=0.6 T and p=2 and 3.

2.6 MHD approximation

The full description of the tokamak plasma would require to solve Botzman's equation for every type of the particles present in the plasma.

$$\frac{\partial f}{\partial t} + v\nabla f + \frac{F}{m}\frac{\partial f}{\partial v} = (\frac{\partial f}{\partial t})_c, \tag{2.17}$$

Here, the $f(v,t)$ is the distribution function of the given type of particles, F represents the total force acting in the system and the term $(\partial f/\partial t)_c$ represents change of the distribution function due to collisions. The full set of Maxwell's equations has to be added to describe mutual interaction of the electromagnetic field and the plasma.

$$\epsilon_0\nabla.E = \sigma, \tag{2.18}$$

$$\nabla \times E = -\dot{B}, \tag{2.19}$$

$$\nabla.B = 0, \tag{2.20}$$

$$\frac{1}{\mu_0}\nabla \times B = j + \dot{E}. \tag{2.21}$$

If gravitation/inertia has to be taken into account, additional equation describing this interaction has to be added.

This treatment is in the most of the cases too cumbersome. Therefore, a simplified approximation called magneto-hydro-dynamic (MHD) is usually applied. [1], [7] The principal simplification is that the equation 2.17 is rewritten so that the unknown parameters are the moments of the distribution function $f(v,t)$ and not the $f(v,t)$ itself. The equation for the first moment is obtained by integration of the equation 2.17 over the whole velocity space. Resulting continuity equation describes flux of the ion or electron mass:

$$\frac{\partial n_{i,e}}{\partial t} + \nabla.(n_{i,e}u_{i,e}) = 0, \tag{2.22}$$

where $n_{i,e}$ is the plasma ions or electrons density, and $u_{i,e}$ is the mean fluid ion or electron velocity. Equation for the second moment of $f(v,t)$ - momentum is obtained by multiplication of equation (2.17) by mv and integration over the whole velocity space. Taking

the force F as the Lorentz force $F = q(E + v \times B)$, one obtains the kinetic fluid equation for the momentum flux:

$$m_{i,e} n_{i,e} [\frac{\partial u_{i,e}}{\partial t} + (u_{i,e}.\nabla) u_{i,e}] = e n_{i,e} (E + u_{i,e} \times B) - \nabla.p_{i,e} + R, \tag{2.23}$$

$p_{i,e}$ has a meaning of pressure tensor and R is the term describing the change of momentum due to collisions. Note, in every equation a one order higher moment of $f(v,t)$ appears. Therefore, following this path of writing the additional equations for the higher moments of $f(v,t)$ we will never obtain a closed system that can be solved. Therefore this system is usually artificially closed by the equation of state for plasma. It is usually supposed that the changes of plasma state are sufficiently faster than dissipation effects, in particular that the heat conductivity is negligible. Hence, changes of state are adiabatic, which can be written as

$$p_{i,e} = C(m_{i,e} n_{i,e})^{\gamma_{i,e}}, \tag{2.24}$$

where C is constant and $\gamma = C_p/C_v$ is the ratio of specific heats.

Equations 2.22, 2.23, 2.24 are written separately for each plasma specie, especially electrons and ions. To describe the plasma in terms of a single magnetized fluid, a new set of variables has to be introduced. They are: fluid density ρ, fluid velocity v and current density j.

$$\rho \equiv \quad n_i M + n_e m \quad \approx n(M+m), \tag{2.25}$$

$$v \equiv \quad \frac{1}{\rho}(n_i M v_i + n_e m v_e) \quad \approx \frac{M v_i + m v_e}{M+m}, \tag{2.26}$$

$$j \equiv \quad e(n_i v_i - n_e v_e) \quad \approx n e(v_i - v_e). \tag{2.27}$$

The kinetic equation of this single magnetized fluid is obtained by summing the kinetic equation written for ions and for electrons according eq. 2.23 using appropriate collision factor and adding a gravitational force $F_g = mg$ that can be generalize to any non electromagnetic force if necessary:

$$M n \frac{\partial v_i}{\partial t} = en(E + v_i \times B) - \nabla.p_i + M n g + P_{i,e}, \tag{2.28}$$

$$m n \frac{\partial v_e}{\partial t} = -en(E + v_e \times B) - \nabla.p_e + m n g + P_{e,i}. \tag{2.29}$$

The resulting kinetic equation is:

$$\rho \frac{\partial v}{\partial t} = j \times B - \nabla p + \rho g. \tag{2.30}$$

The generalized Ohm's law can be obtained by subtracting equations 2.28 and 2.29 in the limit $m/M \to 0$.

$$E + v \times B = \eta j + \frac{1}{en}(j \times B - \nabla p_e) \tag{2.31}$$

The term $j \times B$ is called the Hall current and it can be neglected in many cases as well as the term ∇p_e. The equation of continuity of the mass flux and the charge flux is obtained by adding and subtracting of continuity equation for electrons and ions (eq. 2.22). The resulting set of single fluid MHD equations reads as:

$$\rho \frac{\partial v}{\partial t} = j \times B - \nabla p + \rho g, \tag{2.32}$$

$$E + v \times B = \eta j, \tag{2.33}$$

$$\frac{\partial \rho}{\partial t} + \nabla.(\rho v) = 0, \tag{2.34}$$

$$\frac{\partial \sigma}{\partial t} + \nabla.j = 0. \tag{2.35}$$

$$\tag{2.36}$$

Adding the Maxwell's equations one obtains a relatively simple model of plasma called the MHD fluid model. It supposes the Maxwellian distribution for every plasma specie at every place. If this is not the case, it is necessary to employ the kinetic theory and write and solve the MHD equations for every plasma specie separately. Generally, the fluid MHD theory describes well the phenomena acting primary in perpendicular direction to the magnetic field and it is less efficient for parallel movements. It is because the magnetic field in some sense acts in a similar way as collisions in perpendicular direction and helps to establish the Maxwellian distribution while, it has no effect on particles movement in parallel direction.

2.7 MHD stability of tokamak plasmas – flux functions

The equilibrium magnetic field has to satisfied equation 2.32 with a zero left hand side (time derivative). Neglecting all non-electromagnetic forces one obtains:

$$j \times B = \nabla p \tag{2.37}$$

It is clear from this equation that the magnetic surfaces are the surfaces of constant pressure ($\nabla p \perp B$). Furthermore, it says that the current lines are also bound to the equilibrium magnetic surfaces $\nabla p \perp j$.

In studying tokamak equilibria it is convenient to introduce the poloidal magnetic flux function ψ. The ψ is constant on each magnetic surface and it is defined in cylindrical approximation, where the z axis is along toroidal magnetic field by equations:

$$B_r = -\frac{1}{R}\frac{\partial \psi}{\partial z}, \qquad\qquad B_z = \frac{1}{R}\frac{\partial \psi}{\partial R}. \tag{2.38}$$

The poloidal magnetic flux function is determined by eqs. 2.38 except for the arbitrary additive constant. The current flux function can be defined as well by equations:

$$j_r = -\frac{1}{R}\frac{\partial f}{\partial z}, \qquad\qquad j_z = \frac{1}{R}\frac{\partial j}{\partial R}. \tag{2.39}$$

Using the defined flux functions together with Ampère's the Grad-Schafranov equation can be derived from eq. 2.37.

$$R\frac{\partial}{\partial R}\frac{1}{R}\frac{\partial \psi}{\partial R} + \frac{\partial^2 \psi}{\partial z^2} = -\mu_0 R^2 p'(\psi) - \mu_0^2 f(\psi)f'(\psi). \tag{2.40}$$

This equation is solved numerically to obtain spatial distribution of B_T, j, and p. The typical example of resulting equilibrium magnetic surfaces and profiles is shown in the Fig. 2.7.
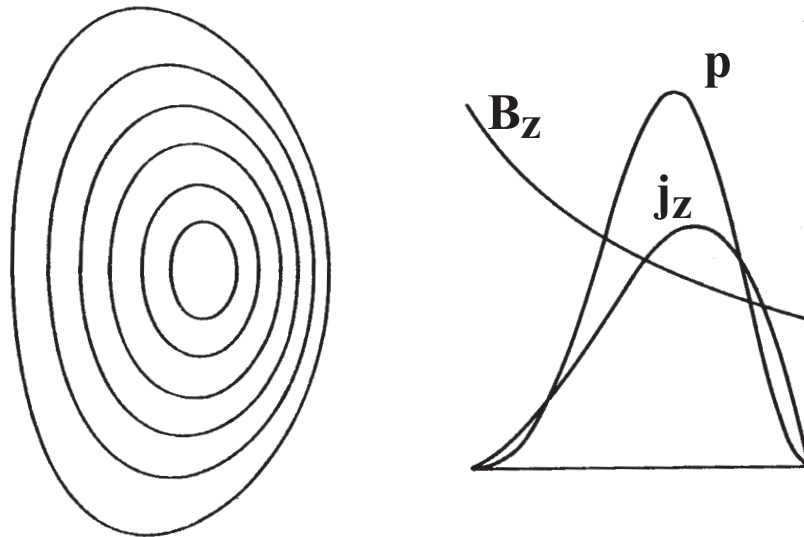
Figure 2.7: Numerical solution of Grad-Schafranov equation. Equilibrium magnetic surfaces - left and equilibrium radial profiles of B_z, j_z, and p - right.

Note the shift of the current density and pressure maximum value from the geometrical center of the current channel. This phenomenon is called Grad-Schafranov shift.

2.8 MHD instabilities in tokamak plasmas

Tokamak plasmas are the fertile soil for a number of different instabilities. [8] Generally, there are two sources of a free energy for the instabilities to grow: nonuniform distribution of the thermal energy and nonuniform distribution of energy of the poloidal magnetic field. The first is given by the plasma pressure gradient while the later by the plasma current density gradient.
 Some instabilities would appear even if the plasma were perfectly conducting. These are called "Ideal MHD instabilities". For other, called "Resistive MHD instabilities", the finite plasma resistivity plays important role.
 Generally, the stabilizing effects are:

- Irrational value of q or, the rational $q = m/n$ with a high mode numbers m, n.
- Favorable curvature of magnetic field lines such that the negative pressure gradient is in the direction of the center of the curvature. The inboard (high field side) of tokamak has the favorable curvature of magnetic field, is more MHD stable, while the outboard (low field side) has unfavorable curvature.

Here, I will mention only the kink instability as a example of the ideal current gradient driven mode and its resistive generalization - tearing modes.

2.8.1 Kink modes

This is a example of ideal MHD instability driven by the current gradient. It is a potentially strongest MHD instability in tokamak plasmas. The intuitive picture of the process can be obtained from the figure 2.8.
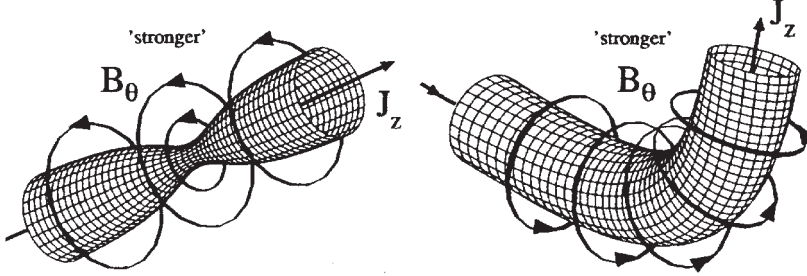

Figure 2.8: Demonstration of the kink mode. The $j_z \times B_\theta$ force tends to further tighten the current channel (left picture) - sausaging, or to further bend it (right) - kinking.

The equation for the kink stability is obtained taking the curl of force balance equation 2.37. Moreover, it is necessary to consider that curl of a gradient is zero and use vector algebra formula $A \times (B \times C) = B(A.C) - C(A.B)$. Following this excercise, one obtains formula:

$$\nabla \times \nabla p = (B.\nabla)j - (j.\nabla)B = 0. \tag{2.41}$$

Using the Ampére's law in cylinder geometry and taking only the radial part of the equation 2.41 results in the final equation of the kink mode stability.

$$\left[\frac{1}{r^2}\frac{\partial}{\partial r}r\frac{\partial}{\partial r}r\tilde{B}_r - \frac{m^2}{r^2}\tilde{B}_r\right] = \frac{\mu_0\frac{\partial}{\partial r}j_0}{B_\theta(1 - \frac{qn}{m})}\tilde{B}_r. \tag{2.42}$$

The left hand side terms represent the stabilizing effect of the magnetic field line bending while the right hand side is the driving term for the instability – current gradient. If the equation holds the kink instability is marginally stable. Note that equation 2.42 has singularity at $q = m/n$ magnetic surface. This problem arises from the assumption of ideal conductivity of plasma. Note also, that the sausage and kink modes shown in the figure 2.8 are corresponding to an m=0 and m=1 modes respectively.

2.9 Tearing modes – magnetic islands

In the vicinity of rational q surfaces the assumption of an ideal MHD breaks down leading to singularity (see eq. 2.42 for $q = m/n$). To improve the model of the current gradient driven MHD instability, a finite plasma resistivity η has to be taken into account using the Ohm's law 2.31. Linearization with respect to the small magnetic perturbation leads to the equation for the tearing mode:

$$\frac{\partial\tilde{B}}{\partial t} = (\dot{B}\nabla)v + \frac{\eta}{\mu_0}\nabla^2\tilde{B}. \tag{2.43}$$

The name tearing modes originates from the fact that close to the rational q surfaces the magnetic field lines tear apart and reconnect as shown in the Fig. **??**. In practice, the equation 2.43 is solved only for the narrow layer around the resonant q surface. The rest of the plasma is described using the ideal MHD approximation. The two results has to be matched afterward, which is not straightforward procedure (see e.g [4]).

Assuming equilibrium, the characteristic width of the magnetic island can be deduced using following procedure. Let's consider a perturbation of equilibrium magnetic field B=(0, B_θ, B_T) in the form (B_r, 0, 0), where:

$$B_r = \hat{B}_r e^{im\chi}, \tag{2.44}$$

and

$$\chi = \theta - \frac{n}{m}\Phi. \tag{2.45}$$

θ and Φ denotes poloidal and toroidal direction respectively. Let's assume that the amplitude of this perturbation is constant over minor radius r. The perturbation in this form grows out of noise level only at radius r_s, where it is in resonance with equilibrium magnetic field line which follows equation:

$$\theta - \frac{1}{q(r_s)}\Phi = const. \tag{2.46}$$

At this resonant magnetic surface laying at radius r_s the poloidal and toroidal magnetic field are related via eq. 2.12 having now the form:

$$q(r_s) = \frac{m}{n} = \frac{r_s}{R}\frac{B_T}{B_\theta(r_s)}. \tag{2.47}$$

Let's first assume a case that an equilibrium magnetic field is in resonance with perturbation given by eq. 2.44 over whole poloidal cross-section. This proposal leads to constant profile of $q(r) = m/n$ ($dq/dr = 0$). Because of favorable conditions, the instability grows rapidly over the whole cross-section and the resulting magnetic field lines finally end at the limiter or in the center of plasma column after several turns. That means that the configuration of magnetic field with constant q profile is inherently unstable.

In the more realistic case the $q(r)$ is not constant and follows eq. 2.12. This situation is depicted in the graphical form in following figure.
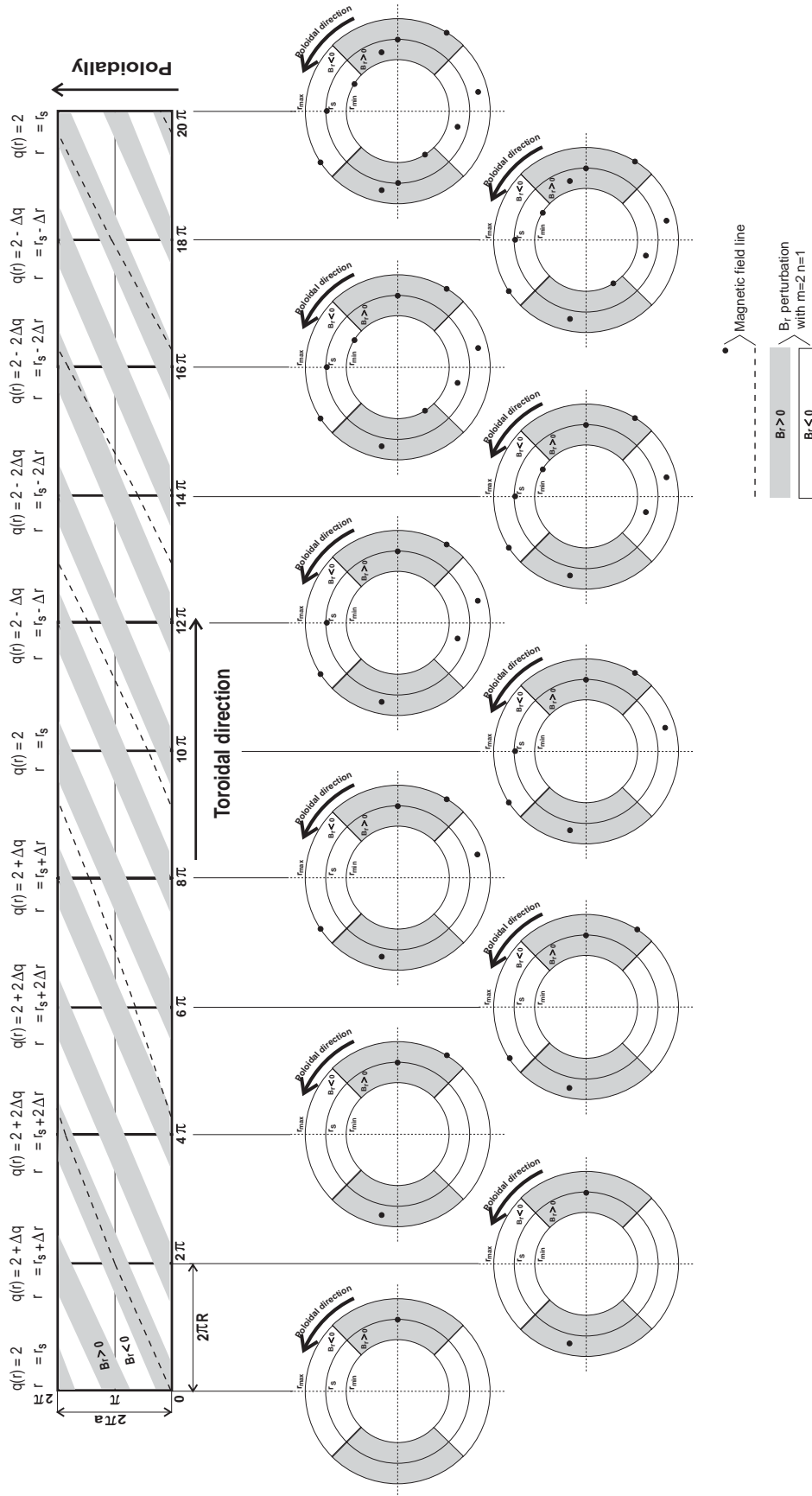
Figure 2.9: Tracking of magnetic field line in presence of B_r perturbation.

Here, the magnetic field line starts at resonant radius r_s in the region with a positive perturbation B_r. Its radial component is increasing and it is shifting outward. However, because of not constant profile of $q(r)$ it simultaneously gets out of resonance with the perturbation. As a result, it moves to the region of negative B_r and starts to return back, inward. This process is continuously repeating and at poloidal cross-section of tokamak a typical picture of magnetic islands appears.

In the following, an equation of perturbed magnetic field line is derived according to [4]. Computation leads to the formula for the width of the magnetic island (radial distance between the most outward and the most inward point which the magnetic field line can reach). We consider the equilibrium configuration around the resonant surfaces having $q(r_s) = q_s = m/n$. The magnetic field lines on this surface define a helix. A perturbation resonant with this surface has the form given by eq. 2.44 where χ is an angular co-ordinate orthogonal to the helix. The equilibrium field in this orthogonal direction is:

$$B_\chi^* = B_\theta(1 - \frac{n}{m}q(r)). \tag{2.48}$$

Using the Taylor expansion of last equation around the resonant surface s and taking into account only the first two terms we obtain:

$$B_\chi^* = -(B_\theta \frac{q'}{q})_s z \tag{2.49}$$

where $z = r - r_s$. The geometry of a magnetic island can be calculated by determining the trajectory of a magnetic field line from the equation

$$\frac{dr}{r_s d\chi} = \frac{B_r}{B_\chi^*}. \tag{2.50}$$

The radial field perturbation may be taken to have the form

$$B_r = \hat{B}_r sin(m\chi). \tag{2.51}$$

Substituting equations (2.49) and (2.51) into equation (2.50), we obtain the differential equation for the magnetic field line in the form

$$-(B_\theta \frac{q'}{q})_s z \ dz = r_s \hat{B}_r sin(m\chi) \ d\chi. \tag{2.52}$$

Taking $\hat{B}_r$ to be essentially constant over the radial extent of the magnetic island, integration of the equation 2.52 gives the equation of the magnetic field line

$$z^2 = \frac{w^2}{8}(cos(m\chi) - cos(m\chi_0)) \tag{2.53}$$

where

$$w = 4\sqrt{(\frac{rq\hat{B}_r}{mq'B_\theta})_s} \tag{2.54}$$

is the width of the magnetic island. χ_0 is the value of χ for which the field line under consideration has $z = 0$. Another important parameter connected with geometry of magnetic field lines is called shear. It is defined as:

$$\hat{s}(r) = \frac{r}{q(r)}\frac{dq(r)}{dr} = 2[1 - \frac{(p+1)(1-\frac{r^2}{a^2})^p \frac{r^2}{a^2}}{1 - (1-\frac{r^2}{a^2})^{p+1}}] \quad . \tag{2.55}$$

The width w of the magnetic island is inversely proportional to $q'/q \sim \hat{s}(r)$. The structure of the magnetic island is shown in figure below.
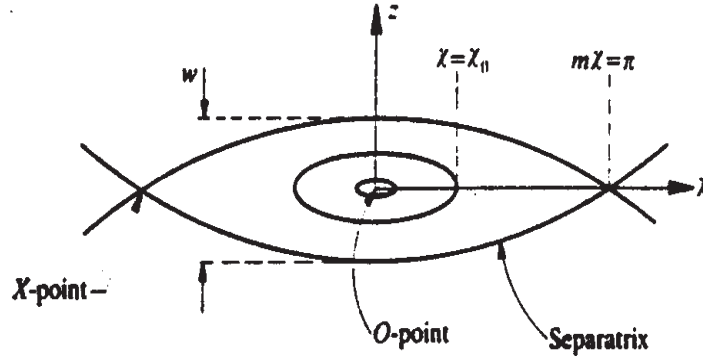

Figure 2.10: *Topology of the magnetic island.*

The magnetic field lines within the magnetic island lie on a set of helical magnetic surfaces with their own magnetic axis. This is labeled the O-point in last figure. The island is bound by the separatrix, the two parts of which meet at the X-points. The distance between the X-points is one full wavelength.

The magnetic islands can be seen as the fluctuations of the radial magnetic field. These fluctuations are usually of the order $B_{fluct}/B_T = 10^{-4}$ in magnitude. This small value causes the great difficulties in all experimental techniques, which deal with them. Nevertheless, these fluctuations seem to play important role in the electron transport. When there is a strong perturbation and magnetic islands on adjacent surfaces are wide enough, they can overlap and the region of nearly stochastic magnetic field is formed. Overlapping of magnetic islands is characterized by overlapping parameter S.

$$S = \frac{w_1 + w_2}{\delta_{12}}, \tag{2.56}$$

where w_1, w_2 are the widths of the adjacent magnetic islands and δ_{12} is their radial distance. The gradual increase of magnetic islands width and formation of stochastic layer is depicted in next figure.
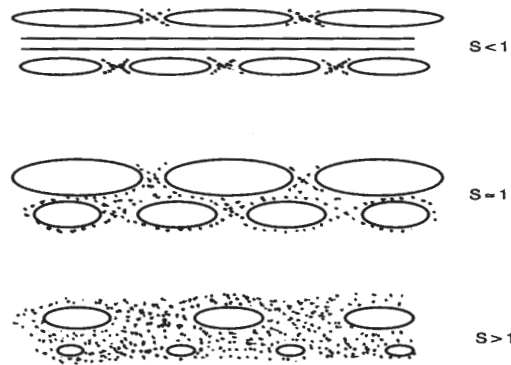
Figure 2.11: *Overlapping of magnetic islands and formation of stochastic magnetic field region.*

According to [6], the onset of ergodization starts for $S = 0.75$. This value implies critical perturbation field:

$$\frac{\tilde{B}_r}{B_T} = 0.3 \cdot \frac{q^2}{Rq'm^3}. \tag{2.57}$$

For $S \geq 1.5$ the magnetic field is supposed to be fully ergodic. In the stochastic region (S>0.75) the radial diffusion is strongly enhanced which substantially increases outflux of especially fast electrons to the walls. This loss of particles can even lead to termination of discharge known as major disruption. Recently, the best theoretical approach to this transport mechanism is Rechester - Rosenbluth formula for collisionless transport in the fully ergodic magnetic field.

2.10 Transport of the electrons across the magnetic field

Classical transport concept assumes ideally nested magnetic flux surfaces as they are displayed in Fig. 2.5(a). It also assumes that the magnetic flux surfaces are isothermals and isobars. The transport is driven by collisions and consequent scattering of the electrons into radial direction. Thus, the transport process is one dimensional from one surface to another with step size of one electron gyro radius. Results of this model don't coincide with experimental values very well. Therefore, the *neoclassical model* was developed. Here, the transport is enhanced due to the curvature and grad-B drift. Further improvement was brought by *anomalous model* of transport. It comes with an idea that the fluctuations of electrostatic field can significantly affect transport of particles through the ExB drift. However, there is still apparent difference between computed and measured transport levels. It seems that the proposal of ideally nested magnetic flux surfaces is oversimplification. In the present state of art it is believed, that the prevailing mechanism of at least fast electrons transport across the magnetic field is diffusion in the *stochastic (ergodic) magnetic field*. This stochastic field is induced by overlapping of magnetic islands. The present best theoretical approach to this mechanism is Rechester - Rosenbluth formula

$$D \sim D_{st}v_{\parallel} \qquad [m^2s^{-1}, m, ms^{-1}] \tag{2.58}$$

where D is diffusion coefficient of the test electron, D_{st} is a diffusion coefficient of field lines, defined as $D_{st} = < (\triangle r)^2 > /2L$, where $\triangle r$ is the radial excursion of the point on the field line, when it travels a distance L along the field line. So the concept is that the magnetic field lines themselves diffuse, and that the particles diffuse because they travel along the field lines. The diffusion coefficient of test particles is proportional to their parallel velocity. This explains the interest for the transport properties of suprathermal electrons. The quasi-linear estimate for D_{st} is given by

$$D_{st} \approx (\frac{B_r}{B_T})^2 L_{c\parallel} \tag{2.59}$$

where $L_{c\parallel}$ is the correlation length along the field lines. When we take $L_{c\parallel} \approx 2\pi R = 2.5m$ and $v_{c\parallel}$ as the typical electron thermal velocity $\approx 10^7 \; m \, s^{-1}$ one obtains that $B_r/B_T \approx 10^{-4}T$ is sufficient to give D of order $1 \, m^2s^{-1}$ which is typical value in tokamaks.

The three major conditions for validity of Rechester - Rosenbluth formula are :

- static stochastic B field

- collisionless test electron

- strong turbulence - field is almost ergodic.

I will discuss here these three basic assumptions which lie at the basis of the Rechester - Rosenbluth formula.

- <u>Static stochastic B field</u> : Typical frequencies of fluctuations of magnetic field in plasma are 10^4 to $10^5 Hz$. Typical collisional frequency of thermal electrons is 10^5 Hz (for $T_e = 1keV$ and $n_e = 3 \times 10^{19} m^{-3}$) and for suprathermal electrons the collisional frequency is even smaller. So, the assumption that a collisionless electron can follow a static field line needs reconsideration : the stochastic field changes while the electron is diffusing.

- <u>Collisionless test electron</u> : This condition mean that the mean free path λ of the electron must be much longer than the correlation length of the field lines $\lambda \gg L_{c\parallel}$. The mean free path of the thermal electron is typically 100 m. The quasi linear estimate yields a short correlation length $L_{c\parallel} \approx R$. However, numerical investigations have shown that the correlation length is at least one order in magnitude longer. In summary, the parallel correlation length may be of the same order as the thermal electron mean free path. This leads to reduction of the diffusivity compared to the Rechester - Rosenbluth formula.

- <u>Strong turbulence - field is almost ergodic</u> : This condition is probably the most debatable. Very rough estimate shows that the fully ergodic field implies the perturbation $B_r/B_T \sim 10^{-2}$ while the observed transport implies $B_r/B_T \sim 10^{-4}$. There is also consistency problem, since the quasi linear estimate is valid only for small perturbation $B_r/B_T \ll 10^{-3}$.

As a result, the validity of the Rechester - Rosenbluth formula is highly debatable, and it should be used with great care. It is at best an upper estimate of the transport coefficient. This also implies that levels of perturbation higher than 10^{-4} may exist in a tokamak without destroying confinement. It is not clear how to do better than the Rechester - Rosenbluth approach. Research is going in the direction of time dependent perturbations of the flux surfaces, which result in a time-varying mix of islands, stochastic layers and ideally nested surfaces. æ

Chapter 3

Diagnostics for measurement of magnetic fields in tokamaks

The chapter gives an overview of diagnostics presently available for measurement of magnetic field in experimental fusion devices. The probe as well as non-perturbing methods are listed. The principles, advantages, and also limitations of these methods are summarized. The emphasis is put on the most commonly used approach - magnetic coils. As a conclusion, the brief perspective for magnetic diagnostics for the ITER tokamak is given.

3.1 Introduction

In tokamaks and stellarators magnetic field $\vec{B}$ with a toroidal shell structure is used to achieve plasma confinement and controlled exhaust. Apparently, it is of principal importance to have information on magnetic field structure with sufficient temporal and spatial resolution. Optimally, this information should be gathered sufficiently fast during the discharge so that it can be used for real time feed-back control of the plasma position, shape, current etc.

The fig. 3.1 shows two examples of a special magnetic field configurations. The right panel shows the plasma shape typical for the stellarator device. Here, the magnetic field is created compleately by external coils in contrast to tokamaks. Therefore, the complicated structure and shape of magnetic coils is necessary as shown in the fig. 3.1. The left panel shows the principal scheme of the divertor concept for the controlled exhaust of particles and energy. Here the additional coils are mounted at the bottom of the tokamak chamber to shape the magnetic field lines in a way such that the plasma can be extracted to the more or less closed divertor structure. The main reason to do this is to localize the plasma-wall interaction within the divertor chamber and to minimize the contamination of the core plasma by the impurities resulting from the plasma-wall interaction.
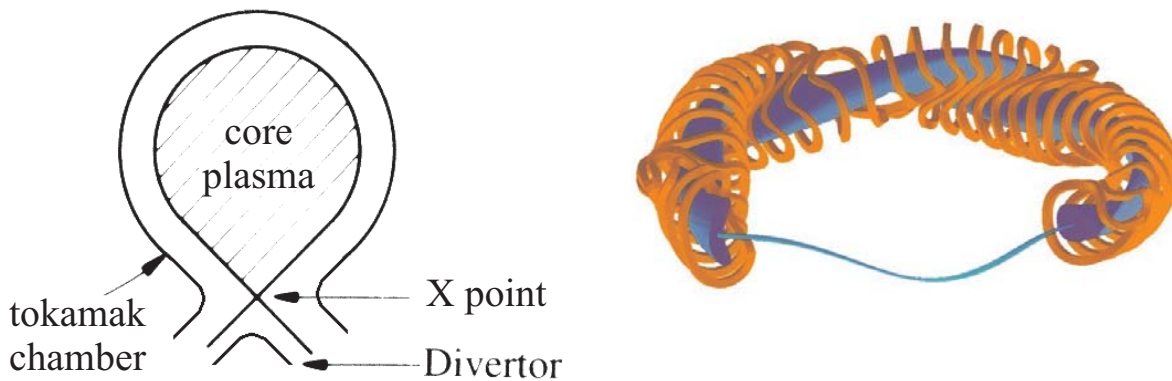

Figure 3.1: Left panel: principal set-up of a tokamak with divertor. Right panel: plasma shape and the configuration of magnetic coils in a stellarator.

There are many experimental methods for measurement of magnetic field. However, only a few of them can be used to determine the local magnetic field inside the hot plasma core of the fusion reactor. In the core plasma the magnetic field can be measured using spectroscopic methods only (Faraday rotation, Motional Stark effect, ...). These measurements are rather difficult. Outside the plasma column or at its very edge, the properly applied probe methods are still acceptable. From measurements of the magnetic fields outside the plasma column many important plasma parameters such as position of plasma column, energy content and consequently energy confinement time, toroidal loop voltage, total plasma current, growth of the MHD (magneto hydrodynamic) modes together with their mode structure and others can be inferred. These measurements have in the past been done using different types of coils. As the time duration of the experiments has increased during the last years, the evaluation of the magnetic field B from the measured

$\dot{B}$ has become more difficult, because the integration needs a precise determination of possible offsets in the preamplifiers, see e.g. [9], [10]. The possible option for the probe diagnostics of B field are the Hall probes. Their output is proportional directly to B but, the temperature and radiation hardness of these semiconductor elements is still the object of active research. In contrast to the present requirements, the temperature resistivity, radiation hardness, excellent reliability, and modularity are the requirements that become critical when considering the magnetic sensors for the future fusion reactor.

3.2 Magnetic coils

Diagnostics based on magnetic coils are presently the standard method for measuring the changes of magnetic field inside fusion plasmas (see e.g. [23], [24], [25]). Turn a piece of wire into a loop and you will obtain the most simple coil for measurement of magnetic field. Increase the number of turns of your coil, or make a larger loop and you will increase its sensitivity. It is that simple. However, as usual, the things get more complicated in a detailed view. The most important requirements which every useful probe must satisfy are:

- reasonable sensitivity, the probe must provide signal high enough to overcome an electric noise usually associated with impulse devices;

- a good frequency response, so as to follow the most rapid fluctuations present in the system;

- minimum perturbing effect on plasma, which means the smallest possible size and appropriate vacuum friendly and plasma resistant construction materials.

It is unfortunate that these requirements conflict directly with each other. It can be seen from the following considerations. Following figure represents the simplified scheme of measuring circuit with the magnetic probe.
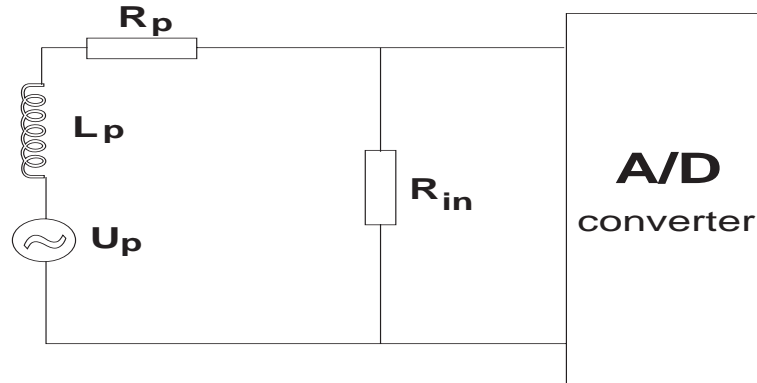

Figure 3.2: Scheme of the measuring circuit.

Here, the voltage source U_p represents the coil output, L_p and R_p are the inductance and resistance of measuring coil and R_{in} is input resistance of digitizer. In standard configuration $R_{in} \gg R_p$. The voltage U_p induced in the coil is according to Faraday law:

$$U_p = -\frac{d\Phi}{dt}, \tag{3.1}$$

where Φ [Wb] is the magnetic flux passing through the coil's cross-section. It is simply related to the magnetic field B [T] by the equation:

$$\Phi = A_{eff}B, \qquad (3.2)$$

where A_{eff} is called effective area of the measuring coil. It is whole area of all turns the coil has. For example, if the coil has n turns arranged in one layer then $A_{eff} = nA$, where A is area of one turn. If turns are arranged in N layers, which is usual, the A_{eff} is given by:

$$A_{eff} = \sum_{i=1}^{N} n_i A_i, \qquad (3.3)$$

where A_i is area of one turn in the i-th layer, and n_i is the number of turns in the i-th layer. Finally, the measured signal V [V] is given by:

$$V = -A_{eff}\frac{dB}{dt}. \qquad (3.4)$$

It is evident from eq. 3.4 that the amplitude of induced voltage increases linearly with the frequency for a given magnetic field amplitude. Finally, the requirement of high output (good sensitivity) implies use of coil with large A_{eff}. That means, coil with large number of turns n but with smallest possible area per turn A to minimize a probe caused perturbation of plasma. The circuit in Fig. 3.2 can be described by the following equation :

$$\frac{d\Phi}{dt} = L_p\frac{dI}{dt} + R_{in}I. \qquad (3.5)$$

It is evident, that the signal registered by the digitizer $V = R_{in}I$ corresponds to the induced voltage U_p only if

$$L_p\frac{dI}{dt} \ll R_{in}I \qquad \text{, or} \qquad \frac{1}{I}\frac{dI}{dt} \ll \frac{R_{in}}{L_p}. \qquad (3.6)$$

The term $\frac{1}{I}\frac{dI}{dt}$ has meaning of maximum frequency correctly registered by the coil. This condition shows that only frequencies $f \ll R_{in}/L_p$ would be correctly measured by the magnetic probe. Hence, the limit of the frequency response is R_{in}/L_p [1]. Considering the dependence of L_p on coil's dimensions, we obtain:

$$f_{max} = \frac{R_i n}{Fn^2 r}, \qquad (3.8)$$

where denominator is coil's inductance in μH. r is coil's radius in cm and F is the constant depending on the ratio of coil length to radius. Then, a reasonable figure of merit for the coil, in the sense of providing the highest output with the best frequency response is product of sensitivity and frequency response, which is to a constant equal to r/n. To make this ratio large requires the biggest possible coil with the smallest number of turns. Therefore, the experimenter is always forced to seek design compromises and there is no general recipe for preparation of coil with satisfactory performance.

---

[1] If, on the other hand $f \gg R_{in}/L_p$ then $I \simeq \Phi/L_p$ and the digitizer monitors

$$V = R_{in}I = \frac{R_{in}}{L_p}\Phi, \qquad (3.7)$$

which is directly proportional to the measured magnetic field (probe works in self integrating mode). Disadvantage of this arrangement is that the output signal is quite low in this case.

3.2.1 Integration of the coil signal

The principal limitations of any diagnostics for measurement of B based on magnetic coils is that the coils measure changes of B and not the B directly. As a result, the stationary B is not detected. For oscillating B the coil's output has to be integrated to be proportional to B.

Analog integration can be performed with the passive (RC-like integrating circuit see Fig. 3.3) or with active elements (transistors,...).
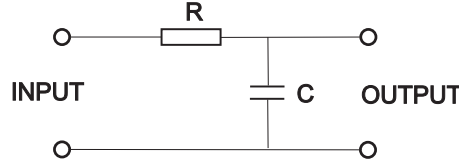

Figure 3.3: The most simple RC analog integrating circuit.

The passive integration is more transparent method but additional circuits lower the output signal significantly. The problem of active integration together with amplification is that the additional active elements complicate the final interpretation of measured data and for longer time periods ($\tilde{1}000$ s) the drifts of integrators present a serious complication.

Another option is to digitize the coils output and perform the integration numerically on computer. According to widespread use of computers as the data processing tools and the high transparency of this method we have always used this mode of operation for our coils. One is of course limited by the finite resolution of the A/D converters.

3.2.2 Electrostatic shielding of the probe versus the skin-effect

Ideally, a magnetic probe should be responsive only to magnetic field, and should be totally insensitive to electrical fields present in the plasma. It is not unusual for a potential difference of several kilovolts to occur between the grounded pickup coil inside the probe jacket and the plasma just outside. The easiest way to overcome this problem is to place a electrostatic shield over the coil. This can have form of cylindrical shell from good conductor. However, due to the skin effect, the penetration of magnetic field lines inside the coil through such electrostatic shield is slowed down. This has negative effect on the coil frequency response. The highest frequency that can be registered by the coil with the cylindrical jacket of radius r, the wall thickness d and the electrical conductivity σ is given by:

$$f_{max} = \frac{2}{\mu r d \sigma}. \tag{3.9}$$

If the effect of electrostatic shielding on frequency response is too severe, the jacket must be slotted which helps the penetration of magnetic field lines toward the coil. This was the case of our coils. Nevertheless, the problems with capacitive coupling of plasma and coil are probably never completely overcame and there is always some uncertainty in this point.

3.2.3 Rogowski coil

Many different kinds of magnetic coil configuration can be used. One which is widely used to measure the electric current is the Rogowski coil. It is a solenoidal coil whose ends are brought around together to form a torus as illustrated in Fig. 3.4.
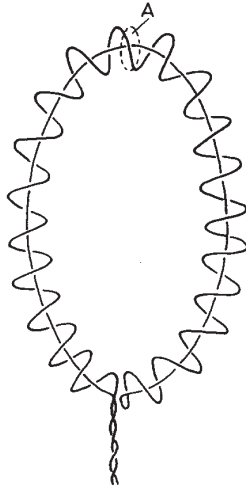

Figure 3.4: The Rogowski coil.

We consider a coil of the uniform cross-sectional area A, with constant turns per unit length - n. Provided the magnetic field varies little over one turn spacing, that is, if

$$|\nabla B|/B \ll n \quad , \tag{3.10}$$

the total flux linkage by the coil can be written as an integral rather than a sum over individual turns:

$$\Phi = n \oint_l dl \oint_A dA \, B \quad , \tag{3.11}$$

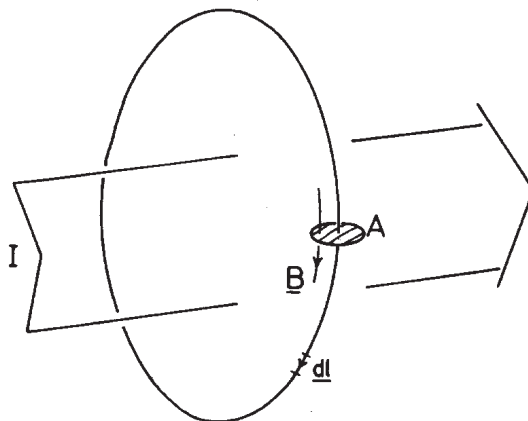where dl is the line element along the solenoidal axis as illustrated in Fig. 3.5.

Figure 3.5: Geometry for the integral form of flux through a Rogowski coil.

Note that it is important to have the return wire back down the coil as shown in Fig. 3.4. Otherwise, eq. 3.11 also includes a term arising from the flux passing through the torus center. Using Amper's law :

$$\oint_l B dl = \mu I, \tag{3.12}$$

where I is the total current encircled by l and μ is the magnetic permeability of the medium in the solenoid, the magnetic flux through the Rogowski coil can be written as:

$$\Phi = nA\mu I. \tag{3.13}$$

The output voltage from the Rogowski coil is according to eq. 3.1 :

$$V = \dot{\Phi} = nA\mu \dot{I}. \tag{3.14}$$

It is seen, that the output voltage from the Rogowski coil is directly proportional to the time derivative of total current flowing through its cross-section. Note particularly that it is independent of the distribution of that current within the loop provided that eq. 3.10 is satisfied.

This principle is used in many different types of electrical circuits since it has the merit of requiring no circuit contact at all with the current being measured. The most common application of Rogowski coil in tokamaks is measurements of toroidal plasma current I_p. The general experimental setup is in the fig. 3.6.
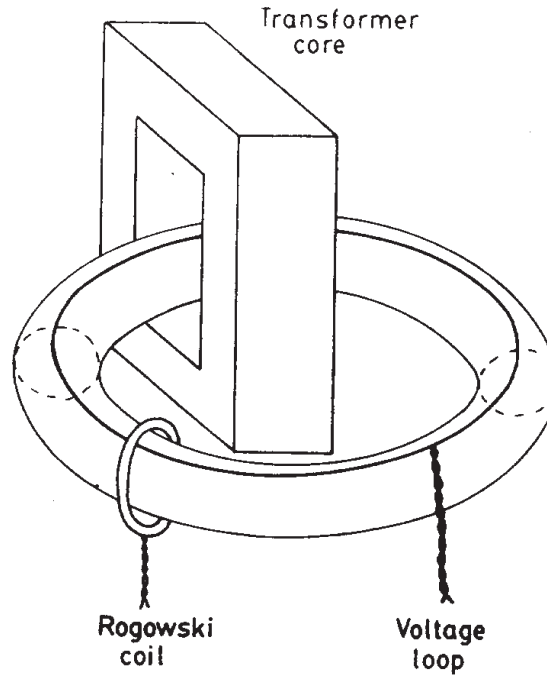

Figure 3.6: Typical use of a Rogowski coil and a voltage loop to measure current and voltage in a toroidal plasma.

In this work the miniature Rogowski coil is used for local measurements of currents in the limiter shadow of the CASTOR tokamak. Its construction is described in Chapter 6 in more details. The fig. 3.6 shows also a principal arrangement of loop measuring the toroidal loop voltage U_{loop}. It is a single toroidal turn of wire paralel to the plasma

column measuring the toroidal electric field $E_T = U_{loop}/(2\pi R)$ induced by transformer action. Knowing the loop voltage and plasma current one can roughly estimate the plasma resistivity by $R_{pl} = U_{loop}/I_p$. Additional magnetic diagnostics that is commonly used in the tokamaks almost from the very beginning is measurement of plasma diamagnetism and consequently the estimation of plasma energy confinement time. This diagnostics technique was described in more details in Chapter 2.

3.3   Hall probes

3.3.1   Introduction

The major draw-back of the use of coils for measuring magnetic field is the necessity to integrate the coil output signal U in order to obtain voltage proportional to B. Another problem, especially in case of measurements inside the plasma column, is the direct relation between the coil's size and it's sensitivity. The coils with larger total area of turns are more sensitive but, because of their size, they cause bigger perturbation of the measuring system.

 The one of the alternative methods for probe measurement of magnetic field are the Hall detectors. These semiconductor elements offer a direct measurement of B with reasonable sensitivity and smaller size than coils, at the cost of more a complicated experimental set-up.

 I would like to kindly ask the reader of this thesis to jump now to Chapter 5 for a brief introduction to the Hall sensors. Please, follow the text for a couple of pages there and then return back and continue with reading of this chapter. Thank you.

3.3.2   Radiation hardness of the Hall sensors

The strongest objection against the use of Hall sensors in the reactor type tokamak is their vulnerability to radiation damage (esp. to the high neutron fluxes). A neutrons (>0.1 MeV) flux density of 2×10^{16} n/(m²s) is expected inside the tokamak fusion reactor ITER vacuum vessel (behind the blanket, where the magnetic sensors will appear) for a possible maximum fusion power of 700 MW [10]. The issue is not as critical as it is for other semiconductor elements as transistors for example. That is because, the physics of transistor is in fact a physics of junction between two types of semiconductors while the Hall effect is a volume process in a single type of a semiconductor. The mechanism of radiation damage is rather simple. The incident neutrons increase the density of the free charge carriers within the volume of the Hall sensor through ionization of semiconductor material. The electric field $\vec{E} = (0, -E_y, 0)$ generated by the Hall effect across the semiconductor inserted into magnetic field $\vec{B} = (0, 0, B_z)$ is given by:

$$\vec{E} = \vec{B} \times \vec{v}. \tag{3.15}$$

The free charge carriers within the semiconductor material are forced to move with velocity $\vec{v} = (v_x, 0, 0)$ by external circuits. The velocity $\vec{v}$ is related to current density $\vec{j}$ by:

$$\vec{j} = ne\vec{v}, \tag{3.16}$$

where e is electric charge of the single free charge carrier in the semiconductor and n is density of the free charge carriers in the semiconductor material. Combining equations

3.15 and 3.16 one obtains:

$$E_y = -\frac{1}{ne}B_z j_x. \tag{3.17}$$

When using the Hall sensors for measurement of magnetic field, the j_x is kept constant by external driving electronic circuits. Consequently, the Hall electric field generated across the Hall sensor is inversely proportional to the density of free charge carriers. Therefore, any ionization process within the sensor decreases its sensitivity.

The existing data on the Hall sensors irradiation tests are sparse and sometimes inconsistent. According to LakeShore Cryogenics, Inc. published also in [11] the 3-5% decrease in sensitivity of highly doped InAs Hall sensors (the most "radiation-hard") was observed after irradiation by 10^{19} n/m^2. That would imply a substantional decrease in sensitivity after 500 s which is a duration of a single ITER (International Thermonuclear Reactor) tokamak discharge. On the other hand, according to [12], and [13] the threshold for "significant damage" to a Hall sensor is in the range $10^{20} - 10^{23}$ n/m^2. That would mean about 5000 discharges (each 1000 s long) in the most optimistic case.

3.4 'Non-standard' diagnostic techniques

In the following, several alternative diagnostic techniques for measurement of magnetic field in the tokamak fusion reactor environment are listed. These approaches are in a different stages of development, offering specific advantages but also limitations. The first six diagnostic techniques are by their nature a probe methods therefore, they can be used only for measurement of magnetic field outside the plasma column or at the very edge. The last three approaches use the spectroscopic means therefore, they can be applied for internal measurements of $\vec{B}$ inside the hot plasma core.

Vibrating or rotating magnetometer

Instead of detecting changes of magnetic field by a fixed coil, it is also possible to measure stationary magnetic field by a coil that moves. However, the frequency and the amplitude of the coil's movement must be known and constant during the whole measurement. This is a major weakness of this technique, because successful long-term operation of such a sensor is highly questionable in a harsh environment of the tokamak fusion reactor.

Magnetostriction

Principle of this method is based on relation between dimensional changes of the probe and the applied magnetic field. The inherent problem is separation of effect of magnetic field from temperature dependence. This can be done by precise temperature stabilization of the probe or better by rotating the probe by angular frequency ω. Then, magnetostrictive effects will appear at harmonics of ω. This method however requires rotation of the probe which immediately rises the questions about its reliability and long-term stability.

Torque magnetometer

There is a torque acting on the magnetized sample when it is not aligned with the external magnetic field. If the magnetization of the sample is stationary, this torque is related to the amplitude and direction of the external uniform magnetic field. This method combines

several disadvantages of the previous ones. There are moving parts and also long-term changes of the sample magnetization will lead to the drift in the measurement.

Turbine

Rotation of a conductor around axis perpendicular to the external magnetic field is slowed down due to an eddy current torque proportional to $kf\sigma B$, where k is constant, f is frequency of the sample rotation, and σ is its conductivity. The decrease of the rotation frequency can be easily measured obtaining the external magnetic field B. Once again, problem of this method is the reliability and stability of the moving parts.

Galvanomagnetic devices

It was found in [14] that the I-V characteristics of an unijunction transistor is modified in a magnetic field. Including such transistor in a relaxation oscillator would result in a change of the oscillator frequency depending on external magnetic field. However, life time of such magnetometer would be very short in any thermonuclear reactor due to the neutron radiation damage.

j×B sensors

Any current channel with current density j inserted inside the magnetic field B is a subject to the $j \times B$ Lorentz force. Driving a constant current through a loop of wire inserted in magnetic field will result in a twist of the loop. This twist is proportional to the external magnetic field. [15] More conveniently, the wire can be bound to the optical fibre. The twist of wire causes slight change of length of the optical fibre that is detected via fiber-optic interferometry. Darkening of the fibres due to neutron damage should be minimized by operating the fibres at high temperatures and in the near infrared wavelength region. Such rather inexpensive device can gain accuracy of 0.0001 % and frequency response up to a hundred Hertz [16], [17].

Faraday rotation

Polarization angle of the laser beam passing through the plasma with the magnetic field B is proportional to $\int nBdl$, where n is the plasma density and dl is the element of the beam path length. In order to unfold the magnetic signal, one must have information about plasma density along the chord. It is usually obtained by interferometry using the same experimental setup. Measurement of density is the major source of problems here, for example, miscounting of phase fringe jumps during rapid plasma transients, false signals due to vibrations, and occasional 'hiccups' of the source laser to mention a few. The time resolution of such polarimeter/interferometer diagnostics is in the 100 microseconds to 10 milliseconds range. [18], [19] Using this principle for measurement of magnetic field externally to the plasma is conveniently done guiding the polarized beam through the optical fibre.

Motional Stark Effect (MSE)

Motional Stark Effect (MSE) diagnostics is successfully working on several tokamaks with neutral beams for internal measurement of magnetic field. [20], [21] It uses the known

velocity of hydrogenic neutral beams and the measured Stark polarization from the $v \times B$ electric field of Balmer transitions to determine the local magnetic field at intersection of the neutral beam and the spectroscopic view. The problems of this method are the low spatial resolution and insufficient accuracy for some application as plasma position control.

Microwave emission (ECE)

It has been suggested that crossed sight-line correlation of the broadband thermal fluctuations in the electron cyclotron radiation could be used to measure the local magnetic field [22] . Accuracy of 0.1% and time resolution of 10 milliseconds for magnetic field 5 Teslas and greater is claimed. A major drawback is that an accurate electron density and temperature information is necessary to unfold the magnetic field.

3.5   Conclusions

In present days, the highest imperative for the fusion community is a successful construction and operation of the ITER tokamak. This device will allow the study of burning plasma physics in the steady state regime ($\tilde{1}000$ s). As a result, the R&D programmes for magnetic diagnostics will be increasingly concentrated on this project.

Several experimental approaches to the measurement of magnetic field, from coils to the 'non-standard' concepts were presented in this chapter. The major task of the magnetic diagnostics for the future steady state fusion reactor is to provide feed-back signal for plasma position control. The most effective solution up to now seems to be the use of flux loops together with integrators. Radiation hardness of such system is limited mostly by stability of cables insulation. Additional, 'real steady state' magnetic field diagnostics is necessary to 'reset' the standard magnetic loops integrator drifts. Here, the most promising candidates are the Hall probes and the $j \times B$ sensors. The radiation hardness of Hall sensors is still in question. Possibility of development of more neutron resistant materials for the Hall sensors might improve prospects of this method. Reliability is the primary problem of the $j \times B$ sensors especially the long term stability of the moving parts.

For internal magnetic field measurements, the MSE and Faraday rotation are already the well established techniques especially for measurement of current density profile. Even though both method offer only a low spatial resolution and complicated experimental setup and interpretation of measured signals, there are not many other options in present. These diagnostics will most probably be included in any future tokamak experimental fusion reactor.

Chapter 4

Magnetic field fluctuations measured on CASTOR tokamak

Measurements of radial magnetic field fluctuations $\tilde{B}_r$ on the CASTOR tokamak are summarized. The array of 8 absolutely calibrated radially oriented pick-up coils is used as a diagnostic tool. Two components of the signal, one corresponding to the broadband microturbulence and the second related to the m=2 magnetic island are identified and studied separately in two geometrical configurations of CASTOR tokamak.

4.1   Introduction

Contents of this chapter is organized in three conference proceedings contributions and one appendix describing the calibration of the diagnostics. The structure of the chapter is as follows:

- The first paper was submitted to proceedings of *IAEA Technical Committee meeting on Research using Small Tokamaks* which took place in Prague in the year 1996. It describes the construction of the array of 8 radial magnetic coils and presents the results of the first measurements on CASTOR. The radial profiles of $\tilde{B}_r$ turbulence level well inside the plasma column is presented for two values of safety factor. The radial correlation length of the magnetic structures is determined.

- My contribution to the diagnostic development laid primary in its absolute calibration. Because, description of the calibration method was over the scope of the previous paper, it is described here in a separate section.

- The second paper was published in proceedings of *Week of Doctoral Students* conference organized by Faculty of Mathematics and Physics in Prague in the year 1997. Here, the additional spectral analysis of the measured magnetic data is presented. The shape of the $\tilde{B}_r$ frequency spectra is found to be related to the safety factor. Comparison with the signals measured by Mirnov coils proved that the spectral peak in $\tilde{B}_r$ signals is a manifestation of the m=2 magnetic structure (magnetic island) rotating within the plasma volume. Radial position of the magnetic island is estimated. The signal components corresponding to the magnetic island and the broadband microturbulence background are numerically separated and treated individually.

- The third paper was published in proceedings of 25th *EPS conference on Plasma Physics and Controlled Fusion* that took place in Prague in the year 1998. In this paper results of measurements for two geometrical configurations of CASTOR tokamak (minor radius equal to 85 mm in the first case and 60 mm in the second) are presented. Stabilizing effect of smaller minor radius was found.

Finally, it was found to be strongly outside the scope of these thesis to answer decisively the question '*What is the importance of magnetic turbulence for the global particle and energy transport in fusion plasmas?*'. If we take the Rechester-Rosenbluth formula, which is the best we have in the present state-of-art, we find that the measured level of $\tilde{B}_r$ turbulence in CASTOR, 0.1 mT in average, yields the particle diffusion coefficient ~ 1 m^2/s. This value is comparable with the transport induced by the electrostatic turbulence in the plasma edge of the CASTOR tokamak. The increasing trend of the level of magnetic turbulence toward the plasma core supports the common opinion that the magnetic turbulence governs the plasma core transport, while the electrostatic fluctuations are responsible for the transport at the plasma edge. As it is clear from the structure of this chapter, I have dedicated the most of my effort to the calibration of the diagnostics and consequently to the understanding and characterization of the magnetic fluctuations under various experimental regimes of CASTOR tokamak. This effort was successful and the amount of knowledge about magnetic turbulence in CASTOR increased substantially.

4.2 Calibration of the magnetic probes array

The absolute calibration of the magnetic probes array was the most important improvement of the existing magnetic diagnostics. In previous experiments, the magnetic fluctuations were measured only in relative units. Therefore, measurements have provided only qualitative information about the magnetic turbulence in the Castor tokamak.
 The output voltage of the coil V is:

$$V = A_{eff} \frac{dB}{dt} \qquad [Volts, m^2, T/s], \qquad (4.1)$$

where A_{eff} =nA is effective area of the coil and dB/dt is the time derivative of the measured magnetic field. The area of one turn is denoted as A and n is the number of turns. That means that the absolute measurement of dB/dt requires a knowledge of the probe effective area A_{eff} which may determined in any of several ways:

- direct geometrical measurement of the coil dimensions,

- measurement of the output voltage when the coil is inserted into a known magnetic field.

We have used the second procedure because it provides the calibration of the entire combination of components used in experiment including electrostatic shielding. A disadvantage of this method is that it requires the accurately known pulsed field to be available. Furthermore, the frequency of this test magnetic field must be close to the experimental one. The previous measurements with uncalibrated probes showed that the typical frequency range of the magnetic perturbations is up to 500 kHz. The natural way to produce such a test field would be to use a Helmholtz coil (produces uniform magnetic field inside the loops) driven by the voltage from transformer. However, the power source with needed frequency range was not readily available, therefore we calibrate the coils in the spatially inhomogeneous magnetic field around the straight conductor as shown schematically in next figure:
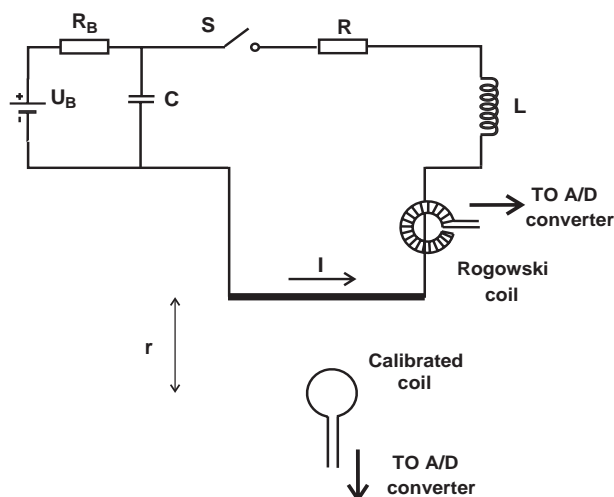

Figure 4.1: Scheme of the calibration circuit.

The basic idea is to use RLC oscillating circuit as the source of the oscillating current, while the frequency of the oscillations is easily tunable by changing the value of the capacitor/inductance in the circuit, according to equation:

$$f = \frac{1}{2\pi}\sqrt{\frac{1}{LC} - \frac{R^2}{4L^2}}. \tag{4.2}$$

The condenser C is charged through resistor R_B up to 50÷100 V. Then the RLC circuit is triggered by the mechanical switch S. The condenser C is discharged through the resistor R (0.2 Ω) and the inductance L (3.9 - 5.6 μH). The maximum frequency of 300 kHz and currents up to 50 A were reached this way. The oscillating current I(t) flows trough the straight thin conductor and it is measured by the absolutely calibrated Rogowski coil operating in a self-integrating regime. The magnetic field at the distance r from the thin conductor was computed according to the Biot-Savart law:

$$B(r,t) = \frac{\mu_0}{2\pi}\frac{I(t)}{r}. \tag{4.3}$$

The time derivative of the magnetic field at distance r produced by current I(t) was measured by the uncalibrated probe. After numerical integration of this signal we have obtained magnetic flux at the distance r from the wire in Voltseconds. The ratio of the measured magnetic flux and the magnetic field computed according to eq. 4.3 yields the effective area of the coil. The calibration was performed at six different frequencies from 5 to 300 kHz. The response of the coil is quite constant (within 5%) for all frequencies used as you can see from following figure.
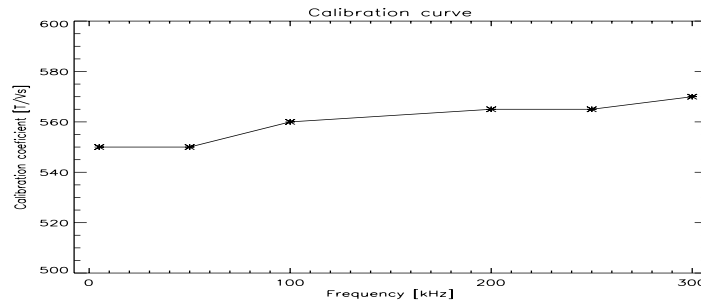

Figure 4.2: Frequency response of a magnetic coil.

The calibration coefficient well corresponds to the value derived from the direct measurement of coil's geometry. It suggests that electrostatic shielding doesn't play any significant role.

Chapter 5

Magnetic field fluctuations measured on TEXTOR tokamak using array of Hall detectors

The results of measurement of magnetic turbulence using array of nine Hall probes in the SOL plasma of the TEXTOR tokamak are summarized within this chapter. The observed phenomena include growth of the m=2 magnetic islands, sawteeth precursors, and decrease of the level of magnetic turbulence during injection of neon to the edge plasmas. Extensive analysis of the diagnostic calibration is presented.

5.1 Introduction

As it was reviewed in Chapter 3, there are several other methods for measurement of magnetic field in fusion devices besides magnetic coils. The development, testing, and using of magnetic diagnostics based on Hall detectors was my primary research interest in the past 3 years.

This chapter summarizes results obtained during my two scientific stays in IPP Jülich on the TEXTOR tokamak. The first stay took place in the spring 2000 and was 2 months long. It was followed by the second stay, one month long, in the autumn of the same year.

The aim of the collaboration between IPP Prague and IPP Jülich was to employ a new diagnostic, array of nine Hall detectors, for measurements of all three components of the magnetic field in the edge plasmas of the TEXTOR tokamak. The diagnostics was developed and put into operation by Dr. Günter Mank from IPP Jülich. As there is a very little experience with the use of Hall probes within the fusion community, the first experiments were primary aimed for testing and exploitation of the diagnostic possibilities in several experimental regimes of TEXTOR. I have developed programs for data analysis based on MATLAB platform in parallel with experimental campaign.

I performed the absolute calibration of the diagnostic in frequency range 1–100 kHz after my return from the first stay in IPP Jülich. The resulting calibration curves allowed recalculation of the measured signals into absolute units. During the second shorter stay we focused on data interpretation and additional supporting measurements.

In the following months I have concentrated on detailed analysis of the calibration measurements. I was puzzled by the appearance of a substantial phase shift between calibration magnetic field and the diagnostic output signal. This phenomena appeared already at ≈ 2 kHz and increased with frequency. It could not be fully explained by nonideal phase characteristics of the measuring electronic circuits (amplifier, filters) therefore, additional mechanism as skin-effect and inductive pick-up had to be introduced. This effort leaded to the publication of the obtained results in *Review of Scientific Instruments, Vol.* **73**, *No. 10, October 2002*. This article summarizes all the obtained results including analysis of the calibration measurements and can be found further in this chapter.

Additional experiments with the Hall probe are planed in 2003, after the TEXTOR with a new Dynamic Ergodic Divertor (DED) for controlled particle and energy exhaust is put into operation. The DED will create a layer of ergodic magnetic field in the edge plasmas [26]. This will enhance edge energy and particle transport and it is supposed to increase the dissipation of the power flux toward the tokamak first wall. If successful, the DED concept might contribute to the solution of the power exhaust from the future fusion reactor.

Figure 5.1: *Left panel demonstrates the configuration of magnetic field lines in TEXTOR with DED. The ergodic layer is formed at the plasma edge. Right panel depicts the installation of DED coils inside the TEXTOR vessel.*
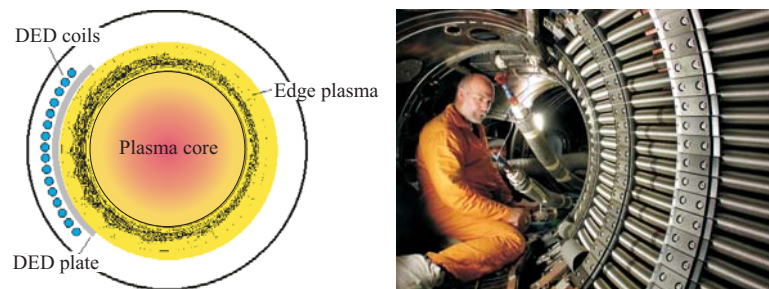
Chapter 6

Link between magnetic and electrostatic turbulence

The chapter addresses a possible relation between electrostatic and magnetic turbulence in the Scrape-off layer (SOL) of tokamaks. The fluctuations of the current flowing parallel to the magnetic field lines are proposed as a missing link between the both in SOL plasmas. Fluctuations of parallel plasma current are studied experimentally on the CASTOR tokamak using a novel probe diagnostic - miniature Rogowski coil combined with a single Langmuir probe tip.

6.1 Introduction

The electrostatic and magnetic turbulence has been extensively studied on the CASTOR tokamak in the last years. In both cases, the rapid changes of the certain plasma parameters, and finally their effect on overall particle and energy balance is studied. Although, it is generally accepted that the turbulence in tokamaks is in its nature electromagnetic, both types of turbulence are studied in most of the fusion machines separately. There are several reasons for that:

- **Different diagnostic tools.** In case of magnetic turbulence, these are primary various configurations of inductive loops. In the last few years, the research at CASTOR is concentrated on implementing novel diagnostic tools, especially Hall probes (see Chapter 5). For study of electrostatic turbulence, various types of Langmuir probes working in different regimes are used. As far as the Langmuir probes are concerned, the CASTOR is probably the best equipped tokamak in the world. Besides advanced Langmuir probes as emissive [27], [28], Gundestrup [29], [30], Mach [31], and tunnel [32], [33], the electrostatic turbulence is monitored with high spatial and temporal resolution by several radial and poloidal arrays of simple Langmuir probes [34]. Furthermore, besides measuring the electrostatic turbulence properties, they are also actively modified and controlled by biasing electrodes inserted into plasma column [35].

- **Different dominant locations.** It is generally recognized, that the magnetic turbulence is dominant for transport of particles and energy within the core plasma while electrostatic turbulence is governing the transport at the plasma edge.

- **Different driving mechanism.** The most of the magnetic instabilities (esp. tearing modes) are driven by current density gradient while the electrostatic turbulence (esp. drift modes) is driven by pressure gradient.

In CASTOR, we looked experimentally for a missing link between electrostatic and magnetic turbulence in the SOL plasmas. According to the Ohm's law, the current density fluctuations are obvious candidate to connect the both.

Within this chapter, three publications are presented that document the progress in this direction.

- The first is the abstract for *IAEA Technical Committee meeting on Research Using Small Tokamaks* taking place in Praha in 1996 (no proceedings of the meeting). It summarizes the status of fluctuations studies performed on the CASTOR tokamak at that time. For the first time, it presents the idea to use miniature Rogowski coil to measure parallel current fluctuations in the SOL of tokamak. It announces also the first experimental results from CASTOR. I was directly involved in preparation of experiments, measurements, and especially data processing and interpretation of results presented in sections *"Magnetic fluctuations in the core plasma"* and *"Link of electrostatic and magnetic fluctuations"* of this abstract.

- The second paper *"Magnetic and electrostatic fluctuations in the CASTOR tokamak"* was published in *Plasma Physics and Controlled Fusion* Vol. 41 (1999) pages A577-A585. It presents a summary of experimental studies of electrostatic (subsection 3.2) and especially magnetic and parallel current fluctuations (subsections 3.1, 3.3, and 3.4) at CASTOR using probe diagnostics.

The principal information from measurements of electrostatic turbulence is that the temporal and spatial structure of these fluctuations in CASTOR and in the SOL of large-scale tokamak experiments is similar. This is the principal motivation for continuation of these studies on CASTOR.

Substantial part of the article is devoted to the magnetic turbulence studies on CASTOR. First, the internal measurements of radial magnetic field fluctuations are briefly summarized in subsection 3.1 (the Chapter 5 of these thesis describes these results in more details). Subsection 3.3 summarizes theoretical expectations resulting from Nedospasov-Endler model of eddies (toroidaly elongated potential and current tubes) in SOL plasmas. We compared these predictions with our experimental observation. The first results of simultaneous measurement of parallel current fluctuations (measured by miniature Rogowski coil) and potential/density fluctuations (measured by a single Langmuir tip) are presented in the subsection 3.4. The first results suggest a rather good agreement with the predictions of Nedospasov-Endler model. The level of parallel current fluctuations reaches the expected value of 1 A/cm^2. Substantially high correlation between the both types of turbulent structures (current–potential/density) is observed in the CASTOR SOL plasmas.

- The third publication *"Longitudinal current fluctuations in the SOL of the CASTOR tokamak"* was published in proceedings of *26th European Physical Society Conference* that took place in Maastricht in 1999. It is dedicated exclusively to the measurement of parallel current fluctuations by miniature Rogowski coil and investigation of validity of Nedospasov-Endler model. The new result presented in the paper is that no switching from correlation to anti–correlation between parallel current and potential fluctuations was observed depending on toroidal position. According to the Nedospasov-Endler model, one sign of the correlation coefficient should be observed near the ion side of the poloidal limiter while the opposite sign should be seen near the electron side. Displacement of plasma column [see e.g ??? Martin thesis] from the center of vacuum chamber is supposed to be responsible for this disagreement.

  The additional new result presented in this publication is the interpretation of the opposite sign of current–potential fluctuations correlation coefficient when the Rogowski coil (RC) is open and closed. According to my idea, this might be caused by finite response of the RC to the current flowing outside its cross-section. The voltage induced in RC by the current channel flowing outside its cross-section has a opposite sign than the voltage induced by the same current channel flowing through the RC cross-section.

To study the influence of the vertical shift of plasma column on magnetic field line topology, I have developed an IDL based program for magnetic field line tracking in the CASTOR tokamak geometry. The arbitrary vertical shift of the plasma column was taken into account. The results of simulation confirmed the idea of crucial importance of precise knowledge of plasma position for interpretation of the discussed correlation measurements. The decisive experiment with a miniature Rogowski coil placed on pendulous holder that would allow to compare measurements at high field side and at low field side of the tokamak chamber in two subsequent shots was proposed. However, due to technical problems this experiment was not realized.

Chapter 7

Experimental validation of two models of electrostatic turbulence

Validity of self-organized criticality (SOC) paradigm for CASTOR tokamak plasmas is experimentally studied using the poloidal and radial arrays of Langmuir probes. Spectral and wavelet analysis is used for statistical analysis of measured data. Results of analytic model of SOL plasmas based on Hasegawa–Wakatani equations is compared with experimental results obtained on CASTOR tokamak.

7.1 Introduction

The effort to understand the transport processes in tokamaks is, unfortunately, still only partially successful. Clearly, a lot of work needs to be done in the theory as well as in experiment. Moreover, probably the most important is a strong collaboration and exchange of results and views between theoreticians and experimentalists on this subject. This chapter contributes to this effort by presenting results of experimental validation of two different models of transport induced by electrostatic fluctuations in the SOL of tokamaks.

- The first article *"Self-Organized Criticality Paradigm"* was published in *Czechoslovak Journal of Physics*, Vol. **50** (2000), Suppl. S3. It presents the idea that the avalanche type of transport (non-diffusive) might be a dominant mechanism of transport at the edge of tokamaks. The self-organized criticality (SOC) state of the system, which allows appearance of avalanches, is manifested by following properties [36]:

  1. The power spectra of the transport events in the system can be divided into several bands, each obeying different power-law [37], [38].

  2. The system has the same statistical properties at all scales – it is self-similar. In another words, the probability distribution function (PDF) of slow events is the same as that of tiny turbulence.

  3. Long term correlation is present in the system. It is manifested by long tails in autocorrelation function.

  The fluctuations of plasma floating potential, ion saturation current and fluctuation induced flux measured in CASTOR SOL plasmas were checked for appearance of the first two of these phenomena. Fluctuations power spectra divided into three bands with different power-law dependencies were clearly identified. However, breaking of self-similarity caused by enhanced wings of PDFs at small scales was observed as well, putting the validity of SOC paradigm for CASTOR plasmas in question. According to the more recent results [36], this breaking of self-similarity might be caused by mixed avalanche-diffusive mode of transport that is supposed to appear in magnetic confinement fusion devices.

- The second article *"Modelling of the effect of the sheared poloidal flow on the electrostatic turbulence on the CASTOR tokamak"* was published in *Czechoslovak Journal of Physics*, Vol. **51** (2001), No. 10. It presents results of model of drift-wave turbulence based on Hasegawa-Wakatani equations [39] accommodated and solved numerically for CASTOR tokamak edge plasmas. This system of equations is combined with an independent fluid model of polarized plasmas to describe the regimes with edge plasma polarization by biasing electrode on CASTOR [40], [41]. Polarization of the edge plasmas enhances shear of poloidal flow and consequently decorrelates turbulent structure which leads to reduction of the edge transport. The results of the model are compared to the edge turbulence properties measured by magnetic coils and Langmuir probes on CASTOR. A good qualitative agreement between the model and experimental observations was reached. The preparation and solving of the model was done by Konstantin Dyabilin from Russia. My contribution

to this effort laid especially in comparison of model results with the experimental observations.

Chapter 8

Summary

The work presented in the thesis is briefly summarized and the main achievements are emphasized within this chapter.

8.1   General remarks

The subject of my doctoral study; organized by department of Electronics and Vacuum Physics, Faculty of Mathematics and Physics, Charles University in Prague; is **"Magnetic fluctuations in tokamak"**. This subject is identical with the one of my diploma thesis [42] therefore, some limited overlap between my diploma and PhD thesis exists. My PhD study started in 1997 and resulted in writing of these theses almost 6 years later in 2003, which is a double of the standard length of doctoral study at Charles University. This prolonged duration was caused mainly by incredible reachness of the subject under study. Also, a lot of possibilities opened in front of me, especially international collaboration in frame of EURATOM including experiments on fusion devices all over Europe as well as international participation in experiments on CASTOR. This brought a lot of new fresh ideas of novel experimental approaches to the study of turbulence in tokamaks and a lot of motivation for their realization. Consequently, less time left for summarizing the results in the thesis. Another reason is that my work was not limited only to the given topic of my study (magnetic turbulence), but it included also some aspects of experimental study of electrostatic turbulence and also modeling. This is partially screened also in the final text and structure of the thesis. Nevertheless, the inability to finish the task in a given time urges me to improve the organization of my work in my future scientific life.
 The thesis are divided into eight chapters:

1. Introduction.

2. Magnetic field in tokamak.

3. Diagnostics for measurement of magnetic fields in tokamaks.

4. Magnetic field fluctuations measured on CASTOR tokamak.

5. Magnetic field fluctuations measured on TEXTOR tokamak using array of Hall detectors.

6. Link between magnetic and electrostatic turbulence.

7. Experimental validation of two models of electrostatic turbulence.

8. Summary.

The first three chapters contain the introduction to the subject of the thesis from the theoretical as well as experimental point of view, while the remaining five chapters present results. The results are presented in the form of already published articles with a short introduction in the beginning of each chapter. This introduction is intended to put the individual publications into the context with the overall headline of the thesis. As all publications have more than one author, I try also to specify my contribution to the work presented. For those articles with myself being the first author, my substantional contribution to the work presented as well as to the preparation of the publication is obvious and sometimes not explicitly specified within the each "Introduction" section.
 In the following, I will briefly summarize the main results contained in the individual chapters 4,5,6, and 7.

8.2 Magnetic field fluctuations measured on CAS-TOR tokamak

The array of 8 absolutely calibrated radially oriented pick-up coils was used to measure fluctuations of radial magnetic field in the edge CASTOR plasmas.

- Measured level of magnetic fluctuations of several militeslas are sufficient to account for particle and energy transport in the CASTOR edge plasmas.

- The structure of measured signals in low q discharges was understood to be a composition of broadband microturbulence and the contribution from m=2 magnetic island poloidally rotating within the core plasmas. The numerical techniques to characterize both of these components separately were developed.

- Stabilizing effect of larger aspect ratio configuration was observed with a factor $\sim$ 3 for both components.

8.3 Magnetic field fluctuations measured on TEX-TOR tokamak using array of Hall detectors

Measurements of magnetic turbulence in SOL of TEXTOR tokamak proved that the Hall effect sensors are a viable option for magnetic field measurements in the tokamak edge plasmas. Compared to conventional option – inductive loops, the Hall sensors present the advantage of smaller size and direct relation of the output signal to the measured magnetic field inductance. The major disadvantage is the low output voltage typically $100\mu V/mT$ and consequently rather high sensitivity to any noise pick-up. The radiation hardness to the high neutron fluxes is in question with respect to the possible use of Hall sensors for monitoring of the steady-state magnetic fields in the future generation of fusion devices. Several interesting phenomena were discovered during measurements on TEXTOR.

- The windowed Fourier transform proved to be a good tool to visualize growth of the MHD modes within the plasma.

- The fine structure of the sawtooth precursors in the time–frequency plane was discovered. This phenomenon is not understood in present and requires additional study and comparison with other diagnostics.

- Decrease of magnetic turbulence during RI regime on TEXTOR (seeding of noble gasses into the edge plasmas) was observed. Additional feature of magnetic signals during RI mode that is not well understood is that the frequency of dominant magnetic perturbation is well correlated with the energy confinement time.

Clearly, several interesting lines for future research appeared. Namely, the tests of radiation hardness of Hall detectors, study of the fine structure of the sawtooth precursors, and understanding of the relation between some features of magnetic signals measured during RI mode with plasma confinement on TEXTOR.

8.4 Link between magnetic and electrostatic turbulence

Miniature Rogowski coil, a new probe diagnostic for local measurement of parallel current density in the edge plasmas was developed and used on CASTOR tokamak to validate Nedospasov-Endler model of current tubes in SOL.

- Levels of parallel current fluctuations of 1 A/cm^2 were measured in SOL plasma for the first time in tokamaks in agreement with the Nedospasov-Endler model.

- Correlation measurements between current and potential fluctuations revealed a significant relationship between current and potential structures (correlation up to 0.5) supporting the Nedospasov-Endler model.

- The precise knowledge of plasma position within the tokamak chamber was understood to be a crucial to correctly interpret the observations that seemingly contradict the model under evaluation.

8.5 Experimental validation of two models of electrostatic turbulence

The radial and poloidal arrays of Langmuir probes were used to test relevance of Self Organized Criticality (SOC) model for CASTOR edge plasmas.

- Three well pronounced frequency bands with a different power law decay are typically observed for frequency power spectra of electrostatic turbulence. This observation supports relevance of Self Organized Criticality (SOC) model for CASTOR edge plasmas.

- The observed breakdown of self-similarity for high frequency microturbulence (>100 kHz) limits the possibility that the SOC induced transport is a single mechanism behind the edge plasma transport and suggests possible mixed SOC/diffusive regime.

The results of model of SOL plasmas based on Hasegawa-Wakatani equations was compared with measurements of parallel current fluctuations done by miniature Rogowski coil and also with spatial/temporal structure of the electrostatic turbulence measured by arrays of Langmuir probes.

- The level of parallel current fluctuations deduced from a model based on Hasegawa-Wakatani model of drift wave turbulence agrees surprisingly well with the measured levels.

- The spatial and temporal structure of potential and density fluctuations agrees well with the experimental observations as well.

- Some discrepancy between the model results and measurement exists in the shapes of electrostatic turbulence frequency spectra.

Appendix A

A.1 Journal publications and scientific reports published in the period 1998–2003

1. F. Žáček, J. Stöckel, L. Kryška, K. Jakubka, J. Badalec, I. Ďuran: Preliminary experiments with edge plasma biasing in tokamak CASTOR, Research Report IPPCZ - 359, March 1998

2. J. Stöckel, J. Badalec, I. Ďuran, J. Horáček, M. Hron, K. Jakubka, L. Kryška, J. Petržílka, F. Žáček, M.V.P. Heller, Z.A. Brazilio and I.L. Caldas: Magnetic and electrostatic fluctuations in the CASTOR tokamak, *Plasma Physics and Control. Fusion*, **41** (1999) A577-A585.

3. F. Žáček, J. Stöckel, L. Kryška, K. Jakubka, J. Badalec, I. Ďuran: Preliminary experiments with edge plasma biasing in tokamak CASTOR, *Czechoslovak Journal of Physics* **48**/S3 (1998), p. 60-72.

4. M. Hron, I. Ďuran, K. Dyabilin, J. Horáček, K. Jakubka, L. Kryška, S. Nanobashvili, J. Stöckel, M. Tendler, G. Van Oost, F. Žáček: Plasma biasing experiments on the CASTOR tokamak, *Czechoslovak Journal of Physics*, Vol. **49** (1999), Suppl. S3, 181-190.

5. I. Ďuran, J. Stöckel, J. Horáček, M. Hron, K. Jakubka, L. Kryška: Self-Organized Criticality paradigm, *Czechoslovak Journal of Physics*, Vol. **50** (2000), Suppl. S3.

6. Gunn J.P., Boucher C., Devynck P., Ďuran I., Dyabilin K., Horacek J., Hron M., Stockel J., Van Oost G., Van Goubergen H., Zacek F.: Edge flow measurements with Gundestrup probes, *Phys. of Plasmas*, Vol. **8**, Number 5 (May 2001), p. 1995-2001.

7. Dyabilin K., Klima R., Ďuran I., Horacek J., Hron M., Pavlo P., Stockel J., Zacek F.: "Modelling of the effect of the sheared poloidal flow on the electrostatic turbulence on the CASTOR tokamak", *Czechoslovak Journal of Physics*, Vol. **51**, No. 10 (October 2001), p. 1107-1117.

8. Gunn J., Stockel J., Adamek J., Ďuran I., Horacek J., Hron M., Jakubka K., Kryska L., Zacek F., Van Oost G.: "Direct measurements of ExB flows and its impact on edge turbulence in the CASTOR tokamak using an optimized Gundestrup probe", *Czechoslovak Journal of Physics*, Vol. **51**, No. 10 (October 2001), p. 1001-1010.

9. Duran I., Stockel J., Mank G., Finken K.H., Fuchs G., Van Oost G., Measurements of magnetic field fluctuations using an array of Hall detectors on the TEXTOR tokamak, *Review of Scientific Instruments*, Vol. **73**, Issue 10, page 3482, October 2002

10. Duran I., Stockel J., Mank G., Finken K.H., Fuchs G., Van Oost G., First results of magnetic turbulence measurements using an array of Hall detectors in the TEXTOR tokamak, *Czechoslovak Journal of Physics*, Vol. **52**, 2002, Suppl. D, D38-D48.

11. Gunn J.P., Devynck P., Pascal J.-Y, Adamek J, Duran I., Hron M, Stockel J, Zacek F, Barina O, Hrach R, Vicher M, Van Oost G, A DC probe diagnostics for fast electron temperature measurements in tokamak edge plasmas, *Czechoslovak Journal of Physics*, Vol. **52**, 2002, 10.

12. Adamek J., Duran I., Hron M., Stockel J., Balan P., Schrittwieser R, Ionota C., Martines E., Tichy M., Van Oost G., Fluctuation measurements with emissive probes in tokamaks, *Czechoslovak Journal of Physics*, Vol. **52**, 2002, No 10, p. 5333C.

13. P. Balan, J. A. Cabral, R. Schrittwieser, H. F. C. Figueiredo, H. Fernandes, C. Ionita, G. Van Oost, J. Adámek, V. Antoni, P. Balan, J.A. Boedo, P. Devynck, I. Ďuran, L. Eliseev, J.P. Gunn, M. Hron, C. Ioni, S. Jachmich, G.S. Kirnev, E. Martines, A. Melnikov, R. Schrittwieser, C. Silva, J. Stöckel, M. Tendler, C. Varandas, M. Van Schoor, V. Vershkov, R.R. Weynants, "Turbulent transport reduction by EB velocity shear during edge plasma biasing: recent experimental results", *Plasma Physics and Controlled Fusion*, Vol. **45**, pages 1–23, 2003.

14. R.A. Pitts, R. Chavan, S.K. Erents, G. Kaveney, G.F. Matthews, G. Neill, J.E. Vince, I. Duran: A retarding field energy analyzer for the JET plasma boundary, *Review of Scientific Instruments*, Vol. **74**, Issue 11, November 2003, pp 4644-4657.

15. R.A. Pitts, R. Chavan, S.K. Erents, G. Kaveney, G.F. Matthews, G. Neill, J.E. Vince, I. Duran: A retarding field energy analyzer for the JET plasma boundary, CRPP EPFL Internal report LRP 765/03, pp 1-35.

A.2   Publications in the Conference proceedings in the period 1998–2003

1. I. Ďuran, J. Stöckel, K. Jakubka: Magnetic turbulence in plasma core of the CASTOR tokamak, proceedings of IAEA Technical Committee Meeting on Research Using Small Fusion Device, Cairo, Egypt, November 1997, published by IAEA as F1-TC-536.13 in Vienna, Austria, 2002, p. 91–96.

2. I. Ďuran, J. Stöckel, K. Jakubka: Coherent modes and broadband magnetic turbulence on the CASTOR tokamak, 1998 ICPP combined with the 25th EPS Conference on Controlled Fusion and Plasma Physics, Prague, Czech Republic, July 1998, p. 714-717.

3. I. Ďuran, J. Stöckel, K. Jakubka: Current density fluctuations measured by miniature Rogowski coil on the CASTOR tokamak, WDS'98, Prague, Czech Republic, June 1998.

4. I. Ďuran, J. Stöckel, K. Jakubka, L. Kryška: Longitudinal current fluctuations in the SOL of the CASTOR tokamak, proceedings of 26th EPS Conference on Controlled Fusion and Plasma Physics, ECA Vol.**23J** (1999), p. 1593 - 1596.

5. I. Ďuran, M. Hron, J. Horáček, K. Jakubka, L. Kryška, J. Stöckel, F. Žáček: Structure of edge turbulence at plasma polarization on the CASTOR tokamak, proceedings of WDS'99, Prague, Czech Republic, June 1999.

6. J. Stöckel, K. Dyabilin, I. Ďuran, J. Horáček, M. Hron, K. Jakubka, L. Kryška, S. Nanobashvili, M. Tendler, G. Van Oost, F. Žáček: Structure of edge turbulence at plasma polarization on the CASTOR tokamak, proceedings of 26th EPS Conference on Controlled Fusion and Plasma Physics, ECA Vol.**23J** (1999), p. 1589-1592.

7. I. Ďuran, J. Stöckel, J. Horáček, M. Hron, K. Jakubka, L. Kryška: Validity of Self-Organized Criticality model for the CASTOR tokamak edge plasmas, proceedings of 27th EPS Conference on Controlled Fusion and Plasma Physics, ECA Vol. **24B**, p. 1693-1696.

8. J. Stöckel, K. Dyabilin, I. Ďuran, J. Horáček, M. Hron, K. Jakubka, L. Kryška, E. Martines, S. Nanobashvili, M. Tendler, G. Van Oost, F. Žáček: Plasma polarization of the separatrix on the CASTOR tokamak, proceedings of 27th EPS Conference on Controlled Fusion and Plasma Physics, ECA Vol. **24B**, p. 1032-1035.

9. Ďuran I., Mank G., Finken K.H., G. Fuchs, A. Kramer-Flecken, G. Van Oost: Measurements of magnetic fluctuations using a multiple Hall probe on TEXTOR, 28th EPS Conference on Controlled Fusion and Plasma Physics, Funchal, Portugal, 18-22 June 2001, ECA Vol. **25A** (2001), p. 1261-1264.

10. Van Oost G., Stockel J., Gunn J., Adamek J., Ďuran I., Horacek J., Hron M., Jakubka K., Kryska L., Zacek F.: "Direct measurements of ExB flows and its impact on edge turbulence in the CASTOR tokamak", 28th EPS Conference on Controlled Fusion and Plasma Physics, Funchal, Portugal, 18-22 June 2001, ECA Vol. **25A** (2001), p. 1665-1668.

11. Dyabilin K., Klima R., Ďuran I., Horacek J., Hron M., Pavlo P., Stockel J., Zacek F.: "Modelling of electrostatic turbulence at the edge of the CASTOR tokamak", 28th EPS Conference on Controlled Fusion and Plasma Physics, Funchal, Portugal, 18-22 June 2001, ECA Vol. **25A** (2001), p. 1669-1672.

12. J. Stockel, J. Gunn, G. Van Oost, I. Ďuran, M. Hron, J. Adamek, J. Horacek, R. Hrach, K. Jakubka, L. Kryska, M. Vicher, F. Zacek: "Optimization of Gundestrup Probe for Ion Flow Measurements in Magnetized Plasmas" 28th EPS Conference on Controlled Fusion and Plasma Physics, Funchal, Portugal, 18-22 June 2001, ECA Vol. **25A** (2001), p. 237-240.

13. Ďuran I., Mank G., Finken K.H., Fuchs G., A. Kramer-Flecken, G. Van Oost: "Magnetic turbulence measurements using array of Hall probes on TEXTOR-94 tokamak", Week of Doctoral Students 2001, Praha, Czech Republic, 12-15 June 2001-11-30 (WDS'01 Proceedings of contributed papers Part II).

14. Hron M., Stockel J., Adamek J., Ďuran I., Horacek J., Jakubka K., Kryska L., Zacek F., Gunn J., Van Oost G.: "Direct measurements of ExB flows and its impact on edge turbulence in the CASTOR tokamak", Week of Doctoral Students 2001, Praha, Czech Republic, 12-15 June 2001-11-30 (WDS'01 Proceedings of contributed papers Part II).

15. Balan P., Adamek J., Ďuran I., Hron M., Ionota C., Martines E., Schrittwieser R., Stockel J., Tichy M., Van Oost G.: Measurements of the fluctuation induced flux with emissive probe in the CASTOR tokamak, 29th EPS conference on Plasma Physics and Controlled Fusion, Montreux, 17-21 June 2002, ECA, Vol. **26B**, P-2-072, (2002).

16. Gunn J.P. Adamek J., Bařina O., Devynck P., Ďuran I., Hrach R., Hron M., Pascal J.-Y., Stockel J., Van Oost G., Vicher M., Žáček F., A DC diagnostics for fast electron temperature measurements in tokamak edge plasma, 29th EPS conference on Plasma Physics and Controlled Fusion, Montreux, 17-21 June 2002, ECA, Vol. **26B**, P-5-093, (2002).

17. Hron M., Martines E., Devynck P., Benhomme G., Gravier E., Adámek J., Doveil F., Voitsekhovitch I., Stockel J., Azeoual A., Ďuran I., Van Oost G., Žáček F., Probe array diagnostics for spatially resolved fluctuation measurements, 29th EPS conference on Plasma Physics and Controlled Fusion, Montreux, 17-21 June 2002, ECA, Vol. **26B**, P-5-043, (2002).

18. Stockel J., Devynck P., Voitsekhovitch I., Adámek J., Azeoual A., Benhomme G., Doveil F., Ďuran I., Gravier E., Hron M., Martines E., Van Oost G., Turbulence and transport with constant and spatial-temporal biasing in the scrape-off layer of CASTOR tokamak, 29th EPS conference on Plasma Physics and Controlled Fusion, Montreux, 17-21 June 2002, ECA Vol. **26B**, O-2-03, (2002).

19. Devynck P, Doveil F., Azeoual A., Voitsekhovitch I., Stockel J., Adámek J., Hron M., Ďuran I., Benhomme G., Gravier E., Martines E., Van Oost G.: Spatial structure of SOL turbulence on CASTOR tokamak, APS Conference, Orlando, Florida USA, Nov. 11-15, 2002, Bull. of Am. Phys. Soc.

20. Stockel J., Devynck P, Voitsekhovitch I., Benhomme G., Martines E., Van Oost G., Adámek J., Azeoual A., Doveil F., Ďuran I., Hron M., Gravier E., Zacek F.: Turbulence and transport with spatial temporal biasing in the scrape-off layer of CASTOR tokamak. I Proc. 19th IAEA Conference on Controlled Fusion, Lyon, October 2002.

21. Gunn J,P, Stöckel J., Adamek J., Balan P., Barina O., Devynck P., Duran I., Hrach R., Hron M., Ionita C., Schrittwieser R., Van Rompuy T., G. Van Oost, Vicher M., Zacek F.: Advances in the measurements and control of tokamak edge turbulence, in Proc 19th IAEA Fusion Energy Conferencs, Lyon, October 2002m poster EX/P1-06.

Bibliography

[1] F.F. Chen: Úvod do fyziky plazmatu, Academia, Praha, 1984.

[2] N.J. Lopes Cardozo, Transactions of fusion technology, Vol. **25**, No. 2T part 2, page 146, 1994.

[3] On the history of the research into controlled thermonuclear fusion, Physics–Uspekhi Fizicheskikh Nauk, Russian Academy of Sciences, **44** (8) 835–865, 2001.

[4] J. Wesson: Tokamaks, Oxford Engineering Science Series, Clarendon Press, Oxford, 1997.

[5] J. Brotánková et al.: Measurement of energy confinement in CASTOR tokamak regimes with edge plasma polarization, Czechoslovak Journal of Physics, Vol. **50**, Suppl. S3, page 75, 2000.

[6] P.H. Rebut, M. Brusati: Magnetic topology, disruptions and electron heat transport, Plasma Physics and Controlled Fusion Vol. **28** No.1A pages 113-124, 1986.

[7] P. Kubeš: Magnetohydrodynamika, Publikace katedry fyziky FEL ČVUT.

[8] P. Ch. de Vries, Magnetic islands in tokamak plasmas, PhD thesis, University Utrecht, The Netherlands, 1997.

[9] G. Fuchs et al., Fusion Eng. Des., Vol. **56–57**, page 711, 2001.

[10] ITER physics expert group on diagnostics et al., Nuclear Fusion, Vol. **39**, page 2541, 1999.

[11] G. Wurden et al.: Steady-state position contreol for the tokamak physics experiment (TPX), 62-940825-LANL, 1997.

[12] J.F. Baur et al.: Radiation hardening of diagnostics for fusion reactor, GA-A16614, 1981.

[13] I. Bolshakova et al.: Novel approaches towards the development of Hall sensor-based magnetometric devices for charged particle accelerators, IEEE Transactions on Applied Superconductivity, Vol. **12**, No. 1, pages 1655–1658, 2002.

[14] S.L. Agrawal et al.: Theoretical analysis of magneto–unijunction transistors, Journal of Physics D – Applied Physics, Vol. **14**, page 283, 1981.

[15] Fujita et al.: Review of Scientific Instruments, Vol. **70** No. 1, 1999.

[16] H. Okamura: Fiber-optic magnetic sensor utilizing metal coated fiber, Electronics Letters, Vol. **23**, No. 16, page 834, 1987.

[17] H. Okamura: Fiber-optic magnetic sensor utilizing the Lorentz force, Journal of Lightwave Tech., Vol. **8**, No. 10, page 1558, 1990.

[18] H. Soltwisch et al.: Current density profiles in the TEXTOR tokamak, Plasma Physics and Controlled Fusion, Vol. **1**, page 263, 1987.

[19] C.H. Ma et al.: Measurements of Faraday rotation in TFTR plasmas, Review of Scientific Instruments, Vol. **57**, page 1994, 1986.

[20] F.M. Levinton: Magnetic field pitch angle diagnostic using the motional Stark effect, Review of Scientific Instruments, Vol. **63** page 5157, 1992.

[21] D. Wroblewski et al.: Polarimetry of motional Stark effect and determination of current profile in DIII-D, Review of Scientific Instruments, Vol. **63** page 5140, 1992.

[22] C.E. Thomas et al.: Crossed–sightline correlation of thermal ECE for remote measurement of absolute magnetic fields, Review of Scientific Instruments, Vol. **63** page 4636, 1992.

[23] R.H. Huddlestone, S.L. Leonard: Diagnostika plazmy, Mir, Moskva, 1967.

[24] D.E. Graessle, S.C. Prager, R.N. Dexter: Q dependence of magnetic turbulence in a tokamak, Phys. Fluids Vol. **B3**, No. 9, 1991.

[25] V. Dhyani: Magnetic fluctuations in CASTOR tokamak, PhD thesis, VOT UFP Praha, 1997.

[26] K.H. Finken: Divertor concept II, Dynamic Ergodic Divertor (DED), Fusion Science and Technology, Vol. **41**, Suppl. T, pages 337–341, 2002.

[27] J. Adamek et al.: Fluctuation measurements with emissive probes in tokamaks, Czech J. Phys, Vol. **52**, No 10, p. 5333C, 2002.

[28] [9] R. Schrittwieser et al.: Measurements with an emissive probe in the CASTOR tokamak, Plasma Phys. Contr. Fusion, Vol. **44**, 567-578, 2002.

[29] J.P. Gunn et al.: Direct measurements of E×B flows and its impact on edge turbulence in the CASTOR tokamak using an optimized Gundestrup probe, Czechoslovak Journal of Physics, Vol. **51**, No. 10, pages 1001–1010, 2001.

[30] J.P. Gunn et al.: Edge flow measurements with Gundestrup probes, Physics of Plasmas, Vol. **8**, No. 5, pages 1995–2001, 2001.

[31] K. Dyabilin et al.: Rotating Mach probe for ion flow measurements on the CASTOR tokamak, Contrib. Plasma Physics, Vol. **1**, No. 1, pages 99–108, 2002.

[32] J.P. Gunn et al.: A DC probe diagnostics for fast electron temeprature measurements in tokamak edge plasmas, Czechoslovak Journal of Physics, Vol. **52**, No. 10, 2002.

[33] J.P. Gunn: Magnetized plasma flow through a small orifice, Physics of Plasmas, Vol. **8**, No. 3, page 1040, 2001.

[34] E. Martines et al.: Coherent structures in the edge turbulence of the Castor tokamak, Plasma Phys. Contr. Fusion, Vol. **44**, pages 351-359, 2002.

[35] J. Stöckel et al.: Turbulence and transport with constant and spatial-temporal biasing in the scrape-off layer of CASTOR tokamak, proceedings of 29th EPS conference on Plasma Physics and Controlled Fusion, Montreux, 17-21 June 2002, ECA, Vol. **26B**.

[36] R. Sanches et al.: Mixed SOC diffusive dynamics as a paradigm for transport in fusion devices, Nuclear Fusion, Vol. **41**, No. 3, page 247, 2001.

[37] D.E. Newman et al.: Sandpile dynamics as a paradigm for turbulent transport, pages. 307-321 in Transport Chaos and Plasma Physics 2, Eds. S. Benkadda, F. Doveil, and Y. Elskens, World Scientific, Singapore, 1996.

[38] M.A. Pedrosa et al.: Empirical Studies of Frequency Spectra of the Edge Plasma Fluctuations in Toroidal Magnetic Confinement Systems, Phys. Rev. Lett. Vol. **82** No. 18, pages 3621-3624, 1999 .

[39] H. Hasegawa, M. Wakatani: Phys. Rew. Lett., Vol. **50**, page 682, 1985.

[40] F. Žáček et al.: Plasma edge biasing on CASTOR tokamak using LHCD, Czechoslovak Journal of Physics, Vol. **51**, No. 10, pages 1129 - 1138, 2001.

[41] G. Van Oost et al.: The role of radial electric fields in the tokamaks TEXTOR-94, CASTOR, and T-10, Czechoslovak Journal of Physics, Vol. **51**, No. 10, pages 957-975, 2001.

[42] I. Ďuran: Fluktuace magnetického pole na tokamaku CASTOR, Faculty of Nuclear Sciences and Physical Engineering, Czech Technical University, Prague, 1997.

Contents